6-2012

Research on Roadway Performance and Distress at Low Temperature

Yong-Rak Kim
University of Nebraska-Lincoln, yong-rak.kim@unl.edu

Soohyok Im
University of Nebraska-Lincoln

Hoki Ban
University of Nebraska-Lincoln

Nebraska Transportation Center

MID-AMERICA TRANSPORTATION CENTER

NDOR Nebraska Department of Roads

Report # MPMC-01

Final Report
26-1121-4004-001

Research on Roadway Performance and Distress at Low Temperature

Yong-Rak Kim, Ph.D.
Associate Professor
Department of Civil Engineering
University of Nebraska-Lincoln

Soohyok Im
Graduate Research Assistant
Hoki Ban, Ph.D.
Postdoctoral Research Associate

2012

Nebraska Transportation Center
262 WHIT
2200 Vine Street
Lincoln, NE 68583-0851
(402) 472-1975

"This report was funded in part through grant[s] from the Federal Highway Administration [and Federal Transit Administration], U.S. Department of Transportation. The views and opinions of the authors [or agency] expressed herein do not necessarily state or reflect those of the U. S. Department of Transportation."

Research on Roadway Performance and Distress at Low Temperature

Yong-Rak Kim, Ph.D.
Associate Professor
Department of Civil Engineering
University of Nebraska–Lincoln

Soohyok Im
Graduate Research Assistant
Department of Civil Engineering
University of Nebraska–Lincoln

Hoki Ban, Ph.D.
Postdoctoral Research Associate
Department of Civil Engineering
University of Nebraska–Lincoln

A Report on Research Sponsored by

Mid-America Transportation Center

University of Nebraska-Lincoln

June 2012

Technical Report Documentation Page

1. Report No MPMC-01	2. Government Accession No.	3. Recipient's Catalog No.	
4. Title and Subtitle Research on Roadway Performance and Distress at Low Temperature		5. Report Date June 2012	
		6. Performing Organization Code	
7. Author/s Yong-Rak Kim, Soohyok Im, and Hoki Ban		8. Performing Organization Report No. MPMC-01	
9. Performing Organization Name and Address University of Nebraska-Lincoln Department of Civil Engineering 362M Whittier Research Center Lincoln, NE 68583-0856		10. Work Unit No. (TRAIS)	
		11. Contract or Grant No. 26-1121-4004-001	
12. Sponsoring Organization Name and Address Nebraska Department of Roads 1500 Hwy. 2 Lincoln, NE 68502		13. Type of Report and Period Covered July 2010–June 2012	
		14. Sponsoring Agency Code MATC TRB RiP No. 26146	
15. Supplementary Notes			
16. Abstract This research project investigated the performance and damage characteristics of Nebraska roadways at low-temperature conditions. To meet the research objective, laboratory tests were incorporated with mechanistic numerical modeling. The three most common pavement structures in Nebraska were selected and modeled considering local environmental conditions and pavement materials with and without truck loading. Cracking of asphalt overlay was predicted and analyzed by conducting finite element simulations incorporated with cohesive zone fracture. Parametric analyses were also conducted by varying pavement geometries and material properties, which could lead to helping pavement designers understand the mechanical sensitivity of design variables on the overall responses and performance characteristics of pavement structures. This better understanding is expected to provide NDOR engineers with more scientific insights into how to select paving materials in a more appropriate way and to advance the current structural pavement design practices.			
17. Key Words Pavement Performance, Low Temperature Cracking, Asphalt, Fracture, Cohesive Zone	18. Distribution Statement		
19. Security Classification (of this report) Unclassified	20. Security Classification (of this page) Unclassified	21. No. of Pages 59	22. Price

Table of Contents

List of Figures

List of Tables

Acknowledgments

The authors thank the Nebraska Department of Roads (NDOR) for the financial support needed to complete this study. In particular, the authors thank the NDOR Technical Advisory Committee (TAC) for their technical support and invaluable discussions/comments.

Disclaimer

The contents of this report reflect the views of the authors, who are responsible for the facts and the accuracy of the information presented herein. This document is disseminated under the sponsorship of the Department of Transportation University Transportation Centers Program, in the interest of information exchange. The U.S. Government assumes no liability for the contents or use thereof.

Abstract

This research project investigated the performance and damage characteristics of Nebraska roadways at low-temperature conditions. To meet the research objective, laboratory tests were incorporated with mechanistic numerical modeling. The three most common pavement structures in Nebraska were selected and modeled considering local environmental conditions and pavement materials with and without truck loading. Cracking of asphalt overlay was predicted and analyzed by conducting finite element simulations incorporated with cohesive zone fracture. Parametric analyses were also conducted by varying pavement geometries and material properties, which could lead to helping pavement designers understand the mechanical sensitivity of design variables on the overall responses and performance characteristics of pavement structures. This better understanding is expected to provide NDOR engineers with more scientific insights into how to select paving materials in a more appropriate way and to advance the current structural pavement design practices.

Chapter 1 Introduction

Roadway performance and distresses at low temperatures have been overlooked in the design of pavement mixtures and structures, even though roadway distresses at low-temperature conditions are the major issues in northern U.S. states. In Nebraska, every year major highways and local gravel roads are subjected to severe low-temperature conditions, followed by the spring thaw. In mid-winter, cracks often develop transversely and longitudinally in local gravel roads. In asphaltic pavements, a number of potholes are created when moisture seeps into the pavement, freezes, expands, and then thaws. As has been well documented, most potholes are initiated due to pavement cracks (by fatigue or thermal) and are exacerbated by low temperatures, as water expands when it freezes to form ice, which results in greater stress on an already cracked road. In this respect, pavement damage and distresses at low temperatures involve extremely complicated processes, which cannot be appropriately identified by merely accounting for the thermal cracking behavior of asphalt binder as the current specifications and pavement design guide handle.

As an example, for the prediction and characterization of low-temperature cracking behavior, the current Superpave specifications and the mechanistic-empirical pavement design guide (MEPDG) are based on the creep and strength data for both asphalt binders and asphalt mixtures. For asphalt binders, two laboratory instruments were developed during the Strategic Highway Research Program (SHRP) to investigate the low-temperature behavior of asphalt binders: the Bending Beam Rheometer (BBR) and the Direct Tension Tester (DTT). For asphalt mixtures, one laboratory-testing device was developed: the Indirect Tension (IDT) Tester. A critical temperature is determined at the intersection between the tensile strength-temperature curve and the thermal stress temperature curve. This approach is used in the thermal cracking

(TC) model, which has been implemented in the MEPDG. The TC model has been regarded as a state-of-the-art tool for performance-based thermal cracking prediction, since the TC model is based on the theory of viscoelasticity, which mechanically predicts thermal stress as a function of time and depth in pavements based on pavement temperatures, which are computed using air temperatures. However, several limitations in the TC model have been identified, such as the use of the simple, phenomenological crack evolution law to estimate crack growth rate, using test results obtained from the Superpave IDT test, which does not accurately identify fracture properties. In addition, the TC model does not consider crack developments related to vehicle loads and environmental conditions; thus, this model cannot fully reflect fracture processes in the mixtures and pavements that are subjected to traffic loading, moisture damage, and low-temperature conditions.

Accordingly, performance and damage characteristics at low-temperature conditions need to be better understood in relation to structural aspects, materials, and environmental conditions together, since the issue is not only load related but also is durability associated.

1.1. Research Objectives and Scope

The primary objective of this research was to investigate the performance and damage characteristics of Nebraska roadways at low-temperature conditions related to the properties of local paving materials, structural design practices of pavements, and locally observed environmental conditions. To meet the objective, laboratory tests were incorporated with mechanistic modeling. Specifically, the three most common pavement structures in Nebraska were selected and modeled considering local environmental conditions (i.e., time- and depth-dependent temperature profile) and pavement materials with and without truck loading. The reflective cracking of the asphalt layer under local conditions was investigated by conducting

finite element analyses incorporated with cohesive zone fracture. Parametric analyses were also conducted by varying pavement geometries and material properties, which would lead to helping pavement designers understand the mechanical sensitivity of design variables on the overall responses and performance characteristics of pavement structures. Consequently, this understanding can better enable engineers to select paving materials in a more appropriate way and to advance the current materials models and performance models at low-temperature conditions.

1.2. Organization of the Report

This report is composed of five chapters. Following this introduction, Chapter 2 summarizes the literature reviews for the modeling of pavement considering thermal effects. Chapter 3 presents the laboratory tests conducted to identify material characteristics at low temperature, including the dynamic modulus test and fracture test. Chapter 4 describes the finite element simulations, of the three most common pavement structures, that were conducted. The simulation results of various cases for parametric analyses are also discussed in the chapter. Finally, Chapter 5 provides a summary of the findings and conclusions of this study. Future implementation plans for NDOR are also presented in the chapter.

Chapter 2 Background

Many researchers have made great efforts to investigate the thermal cracking behavior of asphaltic pavement structures. In order to represent the behavior of pavement structures, such as cracking under thermal loads, it is necessary to examine the thermal cracking mechanism and to incorporate appropriate constitutive material models into these structural mechanistic models. In this chapter, various modeling techniques representing the thermal cracking behavior of pavement structures are described.

2.1. Mechanism of Thermal Cracking

Thermal cracking depends generally on both the magnitude of the low temperature experienced and the cooling rates. Mukhtar and Dempsey (1996) investigated the thermal cracking mechanism of the overlay of asphalt concrete (AC) on Portland cement concrete (PCC) under seasonal temperature changes and daily temperature cycles, as shown in figure 2.1.

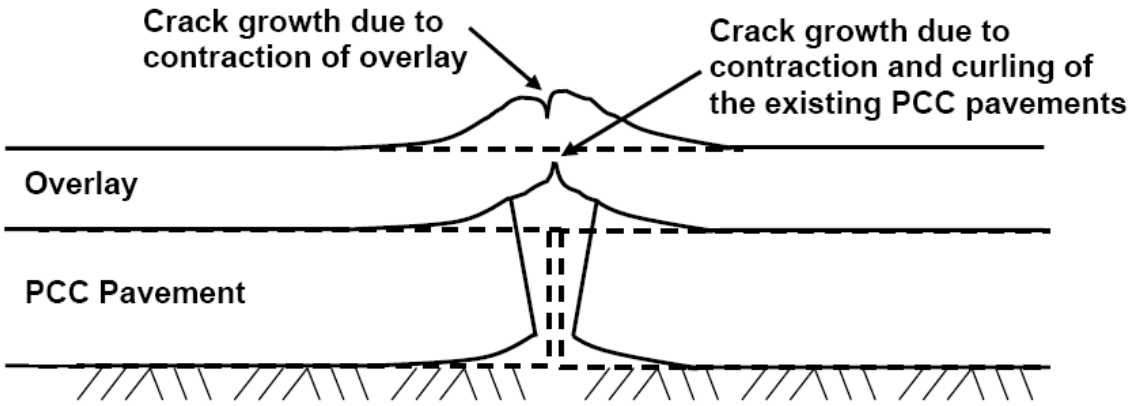

Figure 2.1 Crack propagation in overlay due to temperature changes (Mukhtar and Dempsey 1996)

As depicted in the figure, they reported that due to the temperature cooling down in the evening, the temperature on the surface of the slab is cooler than the bottom of the slab because the effect of the temperature decrease reaches the top of the slab first. The top of the slab contracts, causing the slab to curl upwards and generating tensile stress in the overlay over the joint. Potentially, the combination of the PCC slabs and overlay movements due to temperature differences can cause cracking to initiate from both the top and bottom of the overlay.

2.2. Modeling of Pavement Structures at Low Temperature

Selvadurai et al. (1990) conducted the transient stress analysis of a multilayer pavement structure subjected to heat conduction and associated thermal-elastic effects by the cooling of its surface using finite element analysis. They analyzed the pavement structure behavior at low temperature considering three specific effects: the thickness of the cracked existing asphalt layer, surface crack depth, and the presence of cracks at both the existing asphalt layer and newly paved asphalt layers.

The modeling of reflective and thermal cracking of asphalt concrete was conducted using the cohesive zone model by Dave et al. (2007). Those authors investigated the pavement behavior of an intermediate climate region located at U.S. State Highway 36 near Cameron, Missouri. Although they concluded that the finite element simulations with the cohesive zone model could predict cracking behavior quantitatively, the model validation with field measurement has not yet been provided for use in the study.

Dave and Buttlar (2010) extended their previous study to investigate the thermal reflective cracking of asphalt concrete overlays over PCC and rubblized slab considering different types of mixtures, overlay thickness, and joint spacing of PCC. The authors used the same modeling technique representing thermal cracking behavior as the previous study, which

was cohesive zone fracture modeling. Based on their findings, the overlays over the PCC joints showed bottom-up cracking, while overlays over rubblized slab revealed top-down cracking. However, this may not be accurate because the pavement response to the thermal loading may have been affected by the material properties (i.e., thermal coefficient of asphalt concrete, PCC slab, and rubblized slab and fracture properties of asphalt concrete) as well as the geometry of pavement structures.

Kim and Buttlar (2009) examined the low-temperature cracking behavior of airport pavements under daily temperature change using cohesive zone modeling. To this end, they performed creep compliance tests, indirect tensile tests (IDT), and disk-shaped compact tension (DC[T]) tests to obtain numerical model inputs, such as the viscoelastic and fracture properties of asphalt concrete at low temperature. They reported that two-dimensional fracture models could successfully simulate the crack initiation and crack propagation. Furthermore, the heavy aircraft loading, coupled with thermal loading, had an adverse influence on pavement cracking behavior. However, although the fracture properties are temperature dependent, the fracture properties of -20^{o}C were used in their models.

Souza and Castro (2012) studied the mechanical response of thermo-viscoelastic pavements, considering temperature effect. They used an in-house finite element code, which incorporated the thermo-viscoelastic constitutive model, to investigate the effects of mechanical tire loading, thermal expansion/contraction, and thermo-susceptibility of viscoelastic asphalt materials on the overall pavement responses. Through the various sensitivity analyses, they reported that the deformation and stresses were considerably affected by both thermal deformation and the thermo-susceptibility of the viscoelastic material, individually and together.

Chapter 3 Materials and Laboratory Tests

This chapter presents experimental efforts to characterize the linear viscoelastic and fracture properties of typical asphaltic paving mixtures subjected to various loading rates at different low temperatures. To that end, two laboratory tests − uniaxial compressive cyclic tests to identify the linear viscoelastic properties and semi-circular bending (SCB) fracture tests to characterize the fracture properties − of a dense-graded asphalt concrete mixture were conducted.

3.1. Materials Selection

For the fabrication and testing of the dense-graded asphalt mixture, three aggregates were selected and blended: 16 mm limestone, 6.4 mm limestone, and screenings. All three aggregates were limestone with the same mineralogical origin. The nominal maximum aggregate size (NMAS) of the final aggregate blend was 12.5 mm. Table 3.1 illustrates gradation, bulk specific gravity (G_{sb}), and consensus properties (i.e., fine aggregate angularity (FAA), coarse aggregate angularity (CAA), and flat and elongated (F&E) particles) of the aggregates used in this study. The asphalt binder used in this study was Superpave performance graded binder PG 64-28. With the limestone aggregate blend and the binder, volumetric design of the mixture was performed; this resulted in a binder content of 6.0% by weight of the total mixture to meet the 4.0% target air voids and other necessary volumetric requirements.

Table 3.1 Gradation and properties of aggregates used in this research

Sieve Analysis (Wash) for Gradation										
Aggregate Sources	19mm	12.7mm	9.5mm	#4	#8	#16	#30	#50	#100	#200
16-mm Limestone	100	95	89	-	-	-	-	-	-	-
6.4-mm Limestone	100	100	100	72	-	-	-	-	-	-
Limestone Screenings	100	100	100	10	3	21	14	10	7	3.5
Combined Gradation	100	95	89	72	36	21	14	10	7	3.5
Physical and Geometrical Properties										
Combined Properties	G_{sb} = 2.577, FAA(%) = 45.0, CAA(%) = 89.0, F&E(%) = 0									

3.2. Experimental Programs

Figure 3.1 briefly illustrates the process of sample fabrication and laboratory tests performed for this study. Laboratory tests were conducted to obtain linear viscoelastic properties and to characterize the fracture properties of the mixture. As shown, cylindrical mixture samples were fabricated using a Superpave gyratory compactor (SGC). Two different specimen geometries were extracted from the SGC samples. They were (i) cylindrical cores (150 mm in height and 100 mm in diameter) to be used for determining the linear viscoelastic properties of the mixture and (ii) semi-circular bending (SCB) specimens (150 mm in diameter and 25 mm thick with a 2.5 mm-wide and 25 mm-deep mechanical notch) to be used for fracture tests of the mixture.

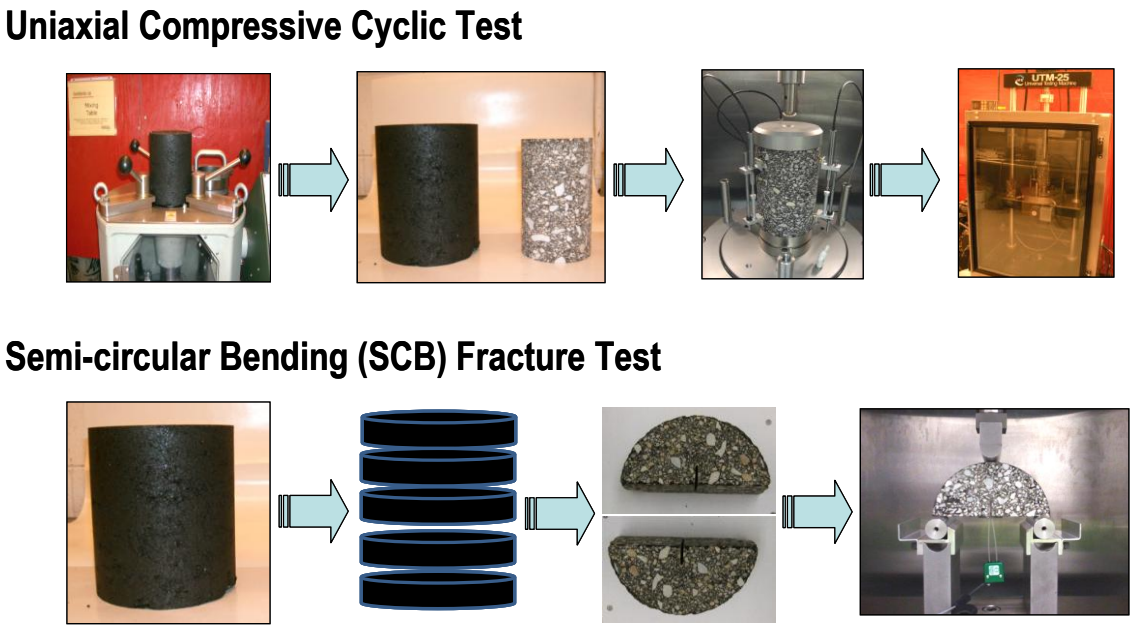

Figure 3.1 Specimen fabrication and laboratory tests performed for this study

3.2.1. Uniaxial Compressive Cyclic Tests for Linear Viscoelastic Properties

Uniaxial compressive cyclic tests were performed for the linear viscoelastic stiffness of the mixture. The loading levels were carefully adjusted until the strain levels were within the range of 0.000050 – 0.000075. Three linear variable differential transformers (LVDTs) were mounted onto the surface of the specimen at 120^{o} radial intervals with a 100 mm gauge length. As suggested in the AASHTO TP 62 (2008), five temperatures (-10, 4.4, 21.1, 37.8, and 54.4^{o}C) and six loading frequencies (25, 10, 5, 1.0, 0.5, and 0.1 Hz) were used, and the frequency-temperature superposition concept was applied to obtain the linear viscoelastic master curves of the storage modulus in the frequency domain for a target reference temperature. The testing results of the storage modulus, as a function of angular frequency, were then fitted with a mathematical function (i.e., Prony series) based on the generalized Maxwell model as follows:

$$E'(\omega) = E_\infty + \sum_{i=1}^{n} \frac{E_i \omega^2 \rho_i^2}{\omega^2 \rho_i^2 + 1} \quad (3.1)$$

where,

$E'(\omega)$ = storage modulus,
ω= angular frequency,
E_∞ = long-time equilibrium modulus,
E_i = spring constants in the generalized Maxwell model,
ρ_i = relaxation time, and
n = number of Maxwell units in the generalized Maxwell model.

Using the Prony series parameters (E_∞, E_i, and ρ_i) obtained by fitting the experimental data with a storage modulus, the relaxation modulus can be expressed in the time domain as follows:

$$E(t) = E_\infty + \sum_{i=1}^{n} E_i e^{-\frac{t}{\rho_i}} \quad (3.2)$$

where,

$E(t)$ = relaxation modulus in time domain, and
t = loading time.

A total of four replicates were tested and the values of the storage modulus at each different testing temperature, over the range of the loading frequencies, were obtained. Figure 3.2 presents the test results. The test results among the replicates at the same testing conditions were generally repeatable without large discrepancies.

The test results from replicates were then averaged to produce 30 individual storage moduli at all levels of temperature and frequency, to produce a stiffness master curve constructed at a reference temperature. The master curve represents the stiffness of the mixture in a wide

range of loading frequencies (or loading times, equivalently). Master curves were constructed using the time (or frequency) - temperature superposition by shifting data at various temperatures, with respect to loading frequency, until the curves merged into a single smooth function. After the shifting was completed, the master curve, at an arbitrary reference temperature, was then fitted with the Prony series (shown in eq. 3.2) to determine linear viscoelastic material parameters. Table 3.2 presents Prony series parameters determined for each different reference temperature. Among them, the Prony series parameters at the reference temperature of -10^{o}C were used for the low temperature-pavement performance simulation in Chapter 4.

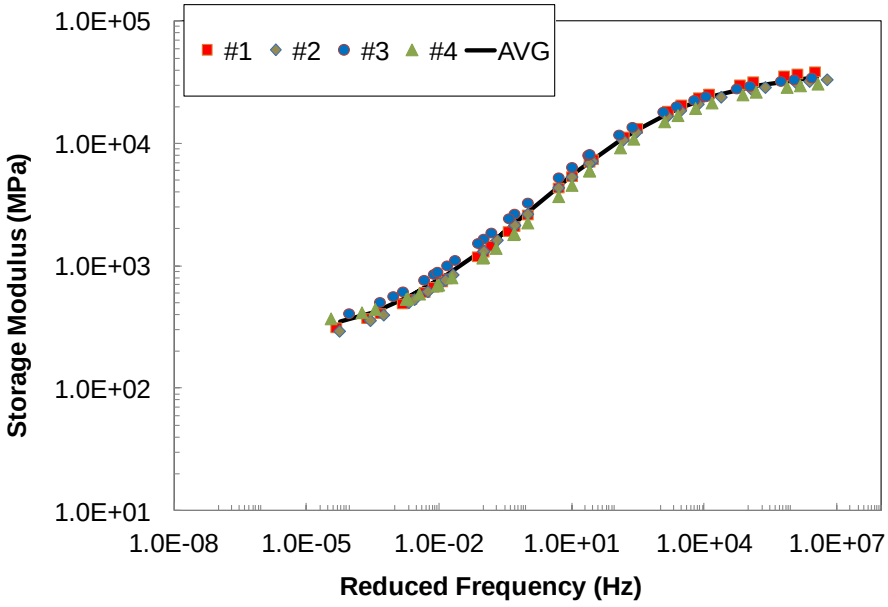

Figure 3.2 Uniaxial compressive cycle test results

Table 3.2 Prony series parameters for each different reference temperature

Reference Temperature	-10°C		0°C		21°C		30°C	
Prony Series Parameters	E_i (MPa)	ρ_i (sec)	E_i (MPa)	ρ_i (sec)	E_i (MPa)	ρ_i (sec)	E_i (MPa)	ρ_i (sec)
1	7391.7	1.0E+00	8095.7	1.0E-01	9095.4	1.0E-05	9028.5	1.0E-05
2	5931.0	1.0E+01	5312.2	1.0E+00	6778.9	1.0E-04	4721.3	1.0E-04
3	6561.0	1.0E+02	4754.5	1.0E+01	7001.4	1.0E-03	4216.1	1.0E-03
4	4526.6	1.0E+03	2243.3	1.0E+02	4250.9	1.0E-02	1879.0	1.0E-02
5	2679.8	1.0E+04	1089.9	1.0E+03	2286.2	1.0E-01	999.9	1.0E-01
6	1238.2	1.0E+05	423.5	1.0E+04	962.4	1.0E+00	397.9	1.0E+00
7	566.9	1.0E+06	203.6	1.0E+05	430.7	1.0E+01	205.7	1.0E+01
8	252.6	1.0E+07	89.8	1.0E+06	186.8	1.0E+02	93.2	1.0E+02
9	124.1	1.0E+08	47.3	1.0E+07	92.8	1.0E+03	52.0	1.0E+03
10	61.0	1.0E+09	23.5	1.0E+08	45.3	1.0E+04	26.2	1.0E+04
11	72.6	1.0E+10	9.1	1.0E+09	53.8	1.0E+05	34.0	1.0E+05
∞	236.1	-	323.7	-	215.3	-	229.5	-

3.2.2. SCB Tests for Fracture Properties

To characterize the fracture properties of asphalt mixtures, researchers in the asphaltic materials and pavement mechanics field have typically pursued four geometries. These are: (i) single-edge notched beam, SE(B), specimen (Mobasher et al. 1997; Hoare and Hesp 2000; Marasteanu et al. 2002); (ii) disc-shaped compact tension, DC(T), specimen (Lee et al. 1995; Wagoner et al. 2005; Wagoner et al. 2006); (iii) semi-circular bending, SCB, specimen (Molenaar et al. 2002; Li and Marasteanu 2004; van Rooijen and de Bondt 2008; Li and Marasteanu 2010; Aragao 2011); and (iv) double-edged notched tension, DENT, specimen (Seo et al. 2002). Among the various options, SCB testing was selected in this study because it has several benefits compared to other fracture test methods. Even if it has some limitations (Wagoner et al. 2005), SCB testing is particularly attractive in that it is very repeatable, simple to perform, and that multiple testing specimens can easily be prepared through a routine process of mixing and Superpave gyratory compacting of asphalt mixtures. Furthermore, the SCB geometry is even more attractive considering the fracture characteristics of field cores, which are usually

circular. Based on these practical benefits, the SCB testing configuration has become a popular geometry for evaluating the fracture behavior of bituminous mixtures.

Before testing, individual SCB specimens were placed inside the environmental chamber of a mechanical testing machine for temperature equilibrium targeting the two different testing temperatures (-10 and 0^{o}C). Following the temperature conditioning step, specimens were subjected to a simple three-point bending configuration with four different monotonic displacement rates (1, 5, 10, and 50 mm/min.) applied to the top center line of the SCB specimens at each testing temperature. Metallic rollers, separated by a distance of 122 mm (14 mm from the edges of the specimen), were used to support the specimen. Reaction force at the loading point and vertical crosshead displacements were monitored by the data acquisition system installed in the mechanical testing machine. A total of 24 SCB specimens were prepared to complete three replicates per test case of the eight test cases in total (four loading rates at two different temperatures).

In an attempt to illustrate the effects of testing conditions on the mixture's fracture behavior, figure 3.3 presents the SCB test results by plotting the average values between the reaction forces and opening displacements at different loading rates and different testing temperatures (i.e., 3.3(a) for -10^{o}C and 3.3(b) for 0^{o}C). At -10^{o}C, although the peak force slightly increases as the loading rate becomes higher, it appears that the fracture behavior is relatively rate-independent, which is typically observed from a linear elastic fracture state. On the other hand, asphalt mixture specimens revealed rate-related global mechanical behavior at 0^{o}C. Slower loading speeds produced more compliant responses than faster cases. Loading rates clearly affect both the peak force and the material softening, which is represented by the shape of the post-peak tailing. The trends presented in figure 3.3 suggest that the rate- and temperature-dependent

nature of the fracture characteristics needs to be considered when modeling the mechanical performance of typical asphalt mixtures and pavements with which a wide range of strain rates and service temperatures is usually associated.

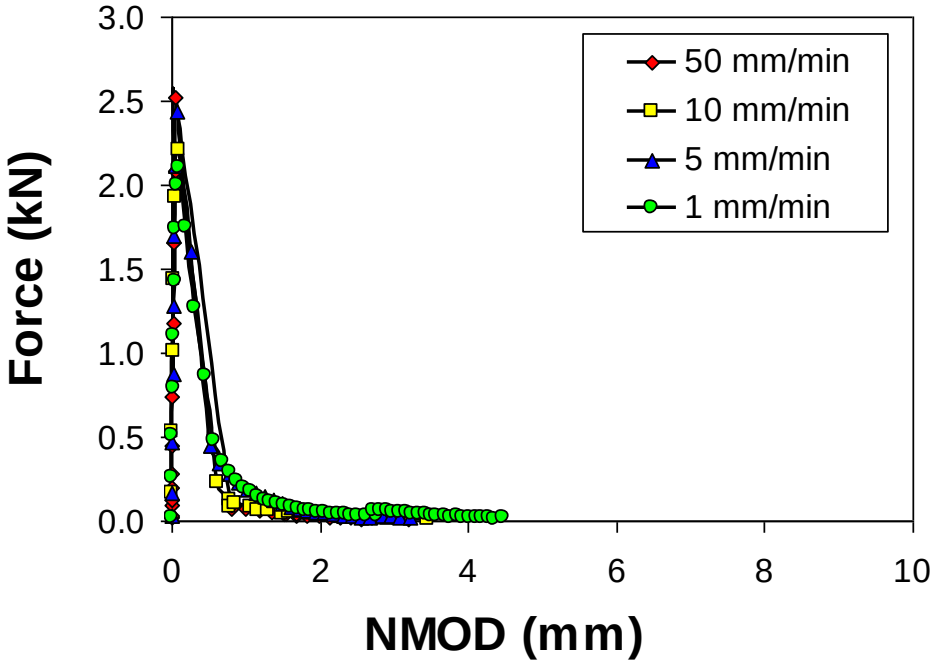

(a) at -10°C

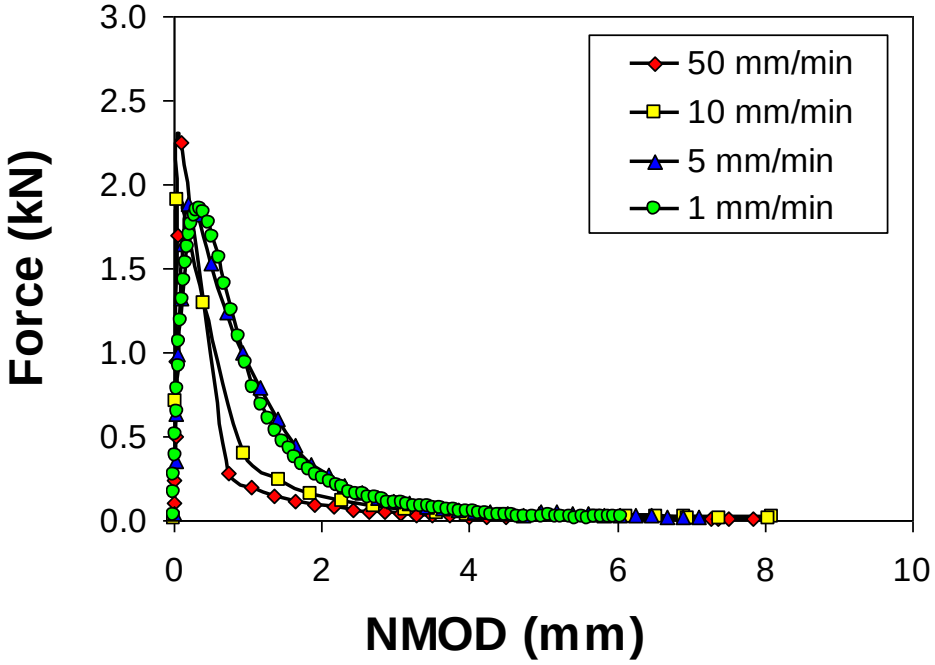

(b) at 0°C

Figure 3.3 SCB test results (force-NMOD) at different loading rates and temperatures

Figure 3.4 presents visual observation of SCB specimens after testing at the two different temperatures. The cracking pattern is presented in figure 3.4(a), and the fracture surfaces of individual specimens are shown in figure 3.4(b). It appears that cracks propagated straight from the crack tip and travelled through the aggregates.

Using SCB test results, the average fracture energy was obtained for each test case. There were several methods (Wagoner et al. 2005; Marasteanu et al. 2007; Song et al. 2008; Aragao 2011) found in the open literature to calculate the fracture energy. Among them, the finite element simulations of the SCB tests, with the cohesive zone model, were conducted to determine the fracture properties that are locally associated to initiate and propagate cracks through the specimens.

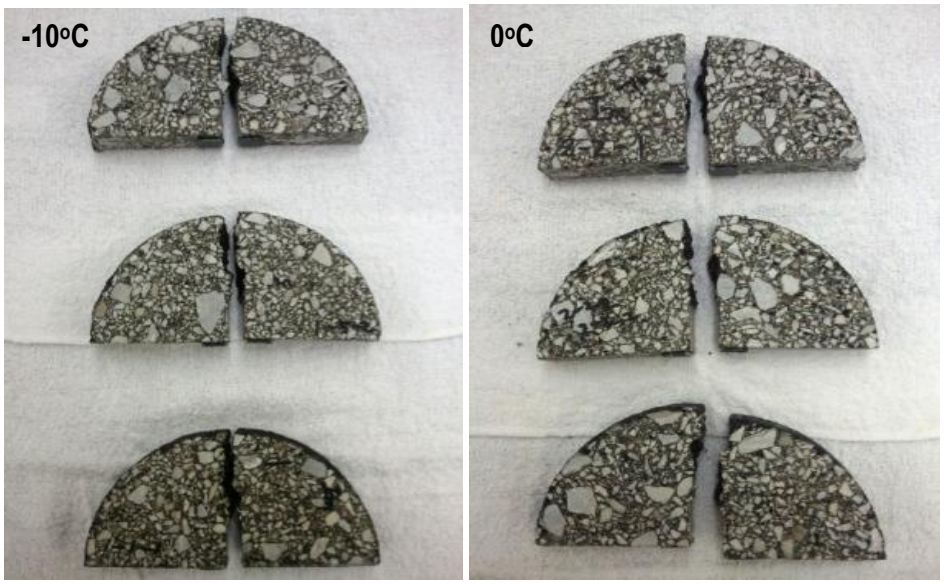

(a) cracking pattern

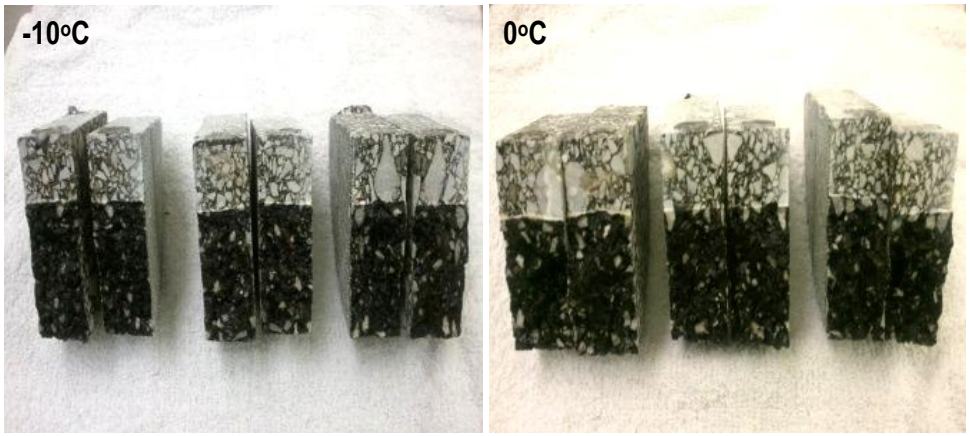

(b) fractured surfaces

Figure 3.4 Visual observation of SCB specimens after testing

The fracture process zone (FPZ) is a nonlinear zone characterized by progressive softening, for which the stress decreases at increasing deformation. The nonlinear softening zone is surrounded by a non-softening nonlinear zone, which represents material inelasticity. Bazant and Planas (1998) skillfully classified the fracture process behavior in certain materials into three types: brittle, ductile, and quasi-brittle. Each type presents different relative sizes of those two nonlinear zones (i.e., softening and non-softening nonlinear zones). Figure 3.5 presents the third

type of behavior, so-called quasi-brittle fracture. It includes situations in which a major part of the nonlinear zone undergoes progressive damage with material softening due to microcracking, void formation, interface breakages, frictional slips, and others. The softening zone is then surrounded by the inelastic material-yielding zone, which is much smaller than the softening zone. This behavior includes a relatively large FPZ, as shown in the figure. Asphaltic paving mixtures are usually classified as quasi-brittle materials (Bazant and Planas 1998; Duan et al. 2006; Kim et al. 2008).

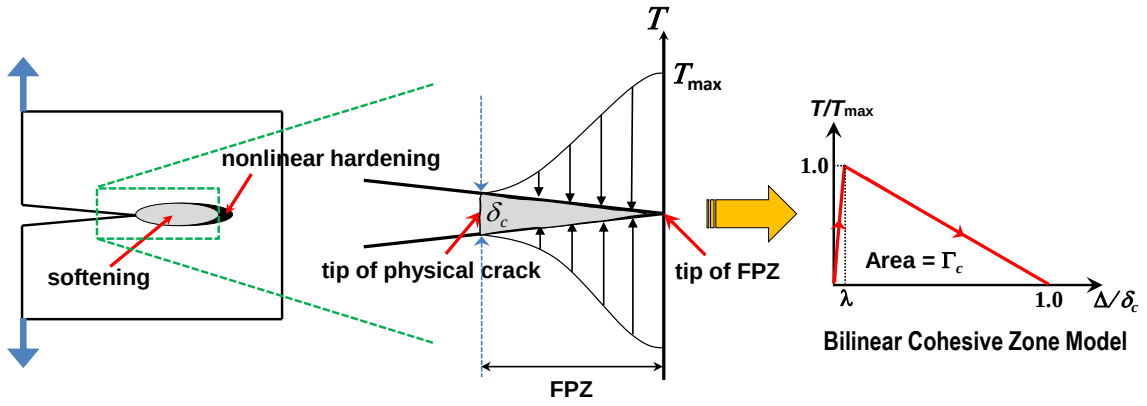

Figure 3.5 Schematic illustration of FPZ of typical quasi-brittle materials

Cohesive zone models regard fracture as a gradual phenomenon in which separation (Δ) takes place across an extended crack tip (or cohesive zone) and where fracture is resisted by cohesive tractions (T). The cohesive zone effectively describes the material resistance when material elements are being displaced. Equations relating normal and tangential displacement jumps across the cohesive surfaces with the proper tractions define a cohesive zone model. Among numerous cohesive zone models developed for different specific purposes, this study used an intrinsic bilinear cohesive zone model (Geubelle and Baylor 1998; Espinosa and

Zavattieri 2003; Song et al. 2006). As shown in figure 3.5, the model assumes that there is a recoverable linear elastic behavior until the traction (T) reaches a peak value, or cohesive strength (T_{max}), at a corresponding separation in the traction-separation curve. At that point, a non-dimensional displacement (λ) can be identified and used to adjust the initial slope in the recoverable linear elastic part of the cohesive law. This capability of the bilinear model to adjust the initial slope is significant because it can alleviate the artificial compliance inherent to intrinsic cohesive zone models. The λ value has been determined through a convergence study designed to find a sufficiently small value to guarantee a level of initial stiffness that renders insignificant artificial compliance of the cohesive zone model. It was observed that a numerical convergence could be met when the effective displacement is smaller than 0.0005, which has been used for simulations in this study. Upon damage initiation, T varies from T_{max} to 0, when a critical displacement (δ_c) is reached and the faces of the cohesive element are separated fully and irreversibly. The cohesive zone fracture energy (Γ_c), which is the locally estimated fracture toughness, can then be calculated by computing the area below the bilinear traction-separation curve with peak traction (T_{max}) and critical displacement (δ_c) as follows:

$$\Gamma_c = \frac{1}{2}\delta_c T_{max} \tag{3.4}$$

Figure 3.6 presents a finite element mesh, which was finally chosen after conducting a mesh convergence study. The specimen was discretized using two-dimensional, three-node triangular elements for the bulk specimen, and zero-thickness cohesive zone elements were inserted along the center of the mesh to permit mode I crack growth in the simulation of SCB testing. The Prony series parameters (shown in table 3.2), determined from the uniaxial

compressive cyclic tests, were used for the viscoelastic elements, and the bilinear cohesive zone model illustrated in figure 3.5, was used to simulate fracture in the middle of the SCB specimen as the opening displacements increased. It should be noted that the simulation conducted herein involves several limitations at this stage by assuming the mixture as homogeneous and isotropic with only mode I crack growth, which may not represent the true fracture process of specimens.

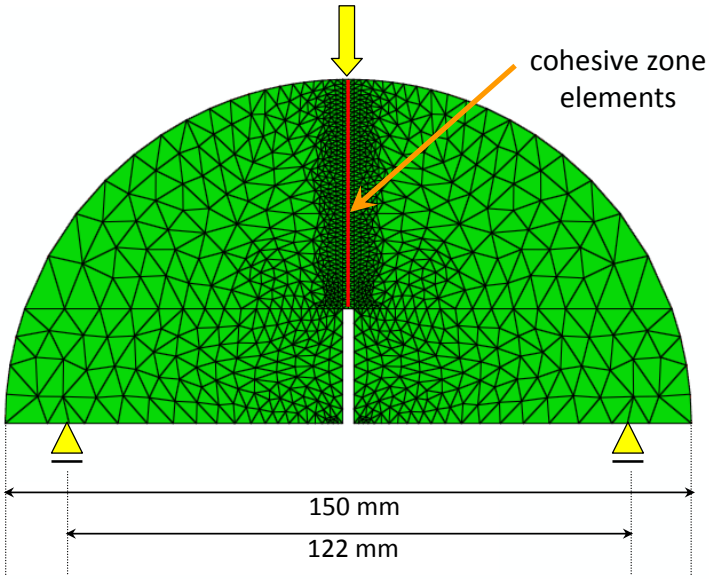

Figure 3.6 A finite element mesh constructed to model the SCB testing

The cohesive zone fracture properties (two independent values of the three: T_{max}, δ_c, and Γ_c) in the bilinear model were determined for each case through the calibration process until a good match between test results and numerical simulations was observed. Figure 3.7 presents a strong agreement between the test results (average of the three SCB specimens) and finite element simulations. Resulting fracture properties (T_{max} and Γ_c) at each different loading rate and testing temperature are presented in table 3.3. The good agreement between tests and model simulations indicates that the local fracture properties were properly defined through the integrated experimental-numerical approach.

Table 3.3 Cohesive zone fracture parameters determined

Temperature (^oC)	Loading Rate (mm/min.)	Cohesive Zone Fracture Parameters	
		T_{max} (kPa)	Γ_c (J/m^2)
-10	1	3.2E+03	350
	5	3.4E+03	350
	10	3.6E+03	350
	50	4.0E+03	350
0	1	2.7E+03	750
	5	2.7E+03	700
	10	3.2E+03	450
	50	3.6E+03	400
	50	6.5E+02	900

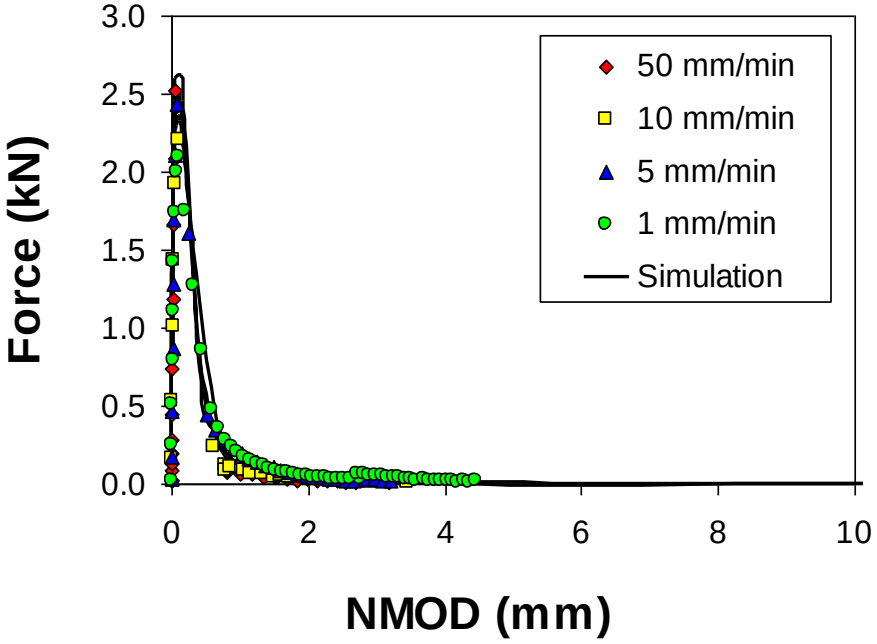

(a) at -10 ^{o}C

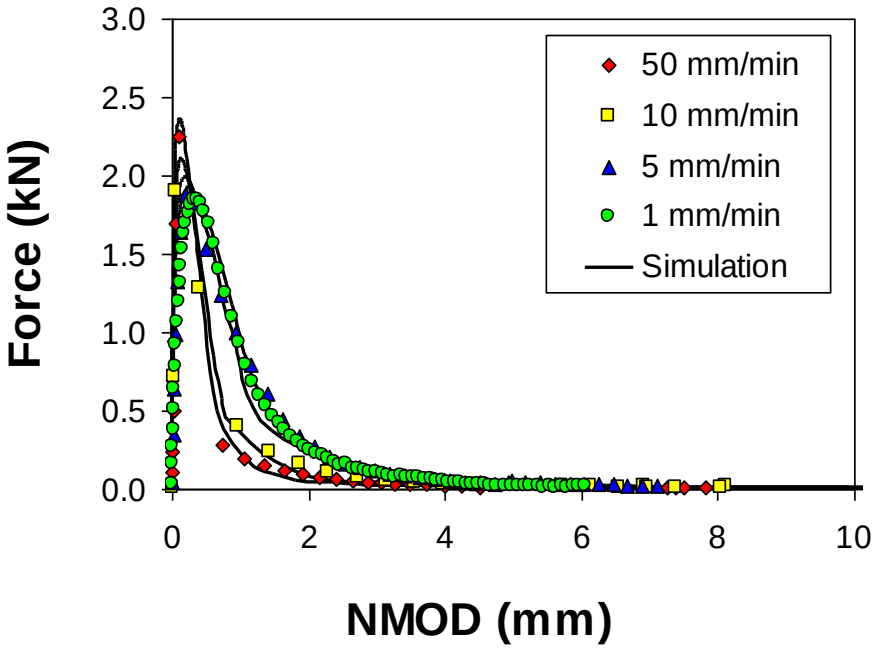

(b) at 0 ^{o}C

Figure 3.7 SCB test results vs. cohesive model simulation results

Chapter 4 Modeling and Simulation Results

In this chapter, the three most common asphaltic pavement structures in Nebraska were modeled through the two-dimensional (2-D) finite element method to investigate the low-temperature performance of the pavements subjected to thermal and mechanical loading. The 2-D finite element modeling was conducted by using a commercial package, ABAQUS version 6.8 (2008), with the mechanical material properties as presented in Chapter 3. The ABAQUS simulation was also incorporated with a user-defined temperature subroutine, UTEMP, to represent effectively the temporal and spatial temperature profile in the pavement structure. The reflective cracking of the asphalt layer was simulated for parametric analyses by varying pavement geometries and layer material properties. This could lead to helping pavement designers understand the mechanical sensitivity of design variables on the overall responses and performance characteristics of pavement structures. Consequently, it can enable engineers to select paving materials in a more appropriate way and to advance the current materials models and performance models at low-temperature conditions.

4.1. Pavement Geometry and Boundary Condition

Figure 4.1 presents the selected asphaltic pavement structures, ST1, ST2, and ST3, which are most commonly observed in Nebraska. As can be seen, ST1 (in fig. 4.1 (a)) includes a new asphalt overlay on a Portland cement concrete (PCC) layer, while ST2 (in fig. 4.1 (b)) and ST3 (in fig. 4.1 (c)) present a new asphalt overlay placed on an existing (old) asphaltic layer. The base and/or subgrade are then located below the PCC or existing asphalt layer. It is noted that all three pavement structures have the same asphalt overlay thickness of four inches (101.6 mm).

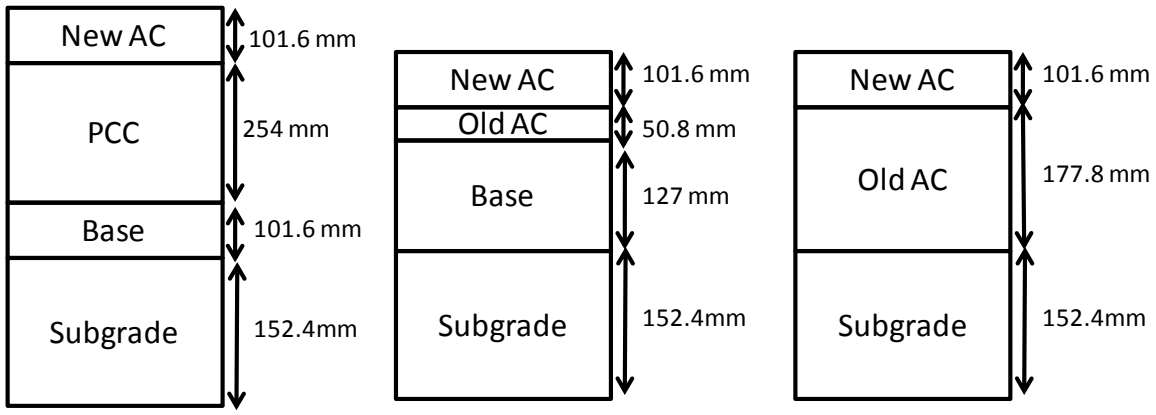

(a) (b) (c)

Figure 4.1 Selected pavement structures: (a) ST1, (b) ST2, and (c) ST3

Among the three pavement structures, figure 4.2 shows a schematic cross-sectional profile of the ST1 and its details of mesh. All finite element simulations in this study were conducted in 2-D along the direction of traffic movement. As illustrated, the pavement structure is repeated with a transverse joint between two PCC slabs. Due to the repeated geometric characteristics, only the 6,000 mm section, where the PCC joint is located in the middle of the section, is necessary for the finite element modeling. The asphalt layer is cracked because of thermal and mechanical loading and the crack is most likely developed from the top of the PCC joint because of high stress concentration. Therefore, cohesive zone elements are embedded through the asphalt overlay along the vertical line of the PCC joint for potential cracking due to thermal effects and/or mechanical truck loading. It can also be noted that the finite element model is constructed with graded meshes, which can reduce the computational time without affecting model accuracy. Graded meshes typically have finer elements close to the high-stress

gradient zone, such as around the PCC joint in this example and coarser elements for the regions of low-stress gradient.

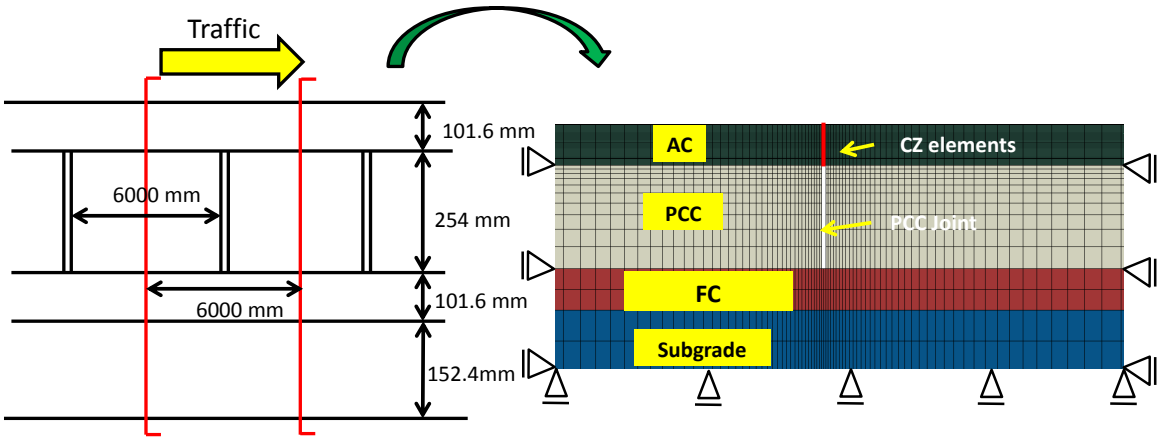

Figure 4.2 Schematic of a finite element model for ST1

Similarly to the modeling of ST1, it was assumed for the modeling of ST2 and ST3 that the existing (old) asphalt layer was fully cracked. The cohesive zone elements were also inserted through the new asphalt overlay along the potential crack path. The same boundary conditions were applied to all three pavement structures. As illustrated in the figure, both sides of the vertical edges were fixed in the horizontal direction, and the bottom of the mesh was fixed in the vertical direction, representing bedrock.

4.2. Governing Equations for the Model

In this study, a thermo-viscoelastic model with cohesive zone fracture was employed for simulating the fracture behavior of the asphalt layer when the pavement was subjected to varying low temperatures and mechanical truck loading. In order to avoid unnecessary complexities at this stage, the inertial effects of the dynamic traffic loads, body forces, and large deformations were ignored, so the problem could be simplified to quasi-static small strain conditions.

It is crucial to select appropriate constitutive models for bulk materials in finite element modeling. For the modeling of underlying layers (i.e., PCC slab, existing old asphalt layer, base, and subgrade), linear thermo-elastic behavior is considered. The linear thermo-elastic constitutive equation can be written as follows:

$$\sigma_{ij}(x_m,t) = C_{ijkl}(x_m)\left\{\varepsilon_{kl}(x_m,t) - \varepsilon^{\theta}_{kl}(x_m,t)\right\} \tag{4.1}$$

$$\varepsilon^{\theta}_{kl}(x_m,t) = \alpha_{kl}(x_m)\left\{\theta(x_m,t) - \theta^{R}(x_m)\right\} \tag{4.2}$$

where,

σ_{ij} = stress tensor,
ε_{kl} = strain tensor,
$C_{ijkl}(x_m)$ = elastic modulus tensor,
α_{kl} = coefficient of thermal expansion,
$\theta(x_m,t)$ = temperature at a particular position and at a certain time,
$\theta^{R}(x_m)$ = stress-free reference temperature, and
x_m = spatial coordinates.

Asphalt concrete material newly placed on top of the PCC slab or an existing old asphalt layer is modeled as linear, thermorheologically simple, and non-aging viscoelastic, with its constitutive equation expressed as follows:

$$\sigma_{ij}(x_m,t) = \int_0^{\xi} C_{ijkl}(x_m,\xi-\tau)\frac{\partial \varepsilon_{kl}(x_m,\tau)}{\partial \tau}d\tau - \int_0^{\xi} \beta_{ij}(x_m,\xi-\tau)\frac{\partial \theta(x_m,\tau)}{\partial \tau}d\tau \qquad (4.3)$$

$$\beta_{ij}(x_m,\xi) = C_{ijkl}(x_m,\xi)\alpha_{kl}(x_m) \qquad (4.4)$$

where,

$C_{ijkl}(x_m,\xi)$ = thermo-viscoelastic relaxation modulus tensor,
$\beta_{ij}(x_m,\xi)$ = second-order tensor of relaxation modulus relating stress to temperature variations,
ξ = reduced time, and
τ = time integration variable.

The reduced time can be defined as follows:

$$\xi(t) \equiv \int_0^{t} \frac{1}{a_T(\theta(\tau))}d\tau \qquad (4.5)$$

where,

t = real time, and
a_T = temperature shift factor.

The temperature shift factor, $a_T(\theta(t))$, is generally described by either the Arrhenius or the WLF equations (Williams et al. 1955). In the present study, the shift factor is described according to the WLF equation:

$$\log_{10}(a_T) = \frac{-C_1(\theta-\theta^R)}{C_2+(\theta-\theta^R)} \qquad (4.6)$$

where,

C_1, C_2 = model constants.

The thermo-viscoelastic relaxation modulus of asphalt concrete is determined by performing laboratory tests, such as dynamic frequency sweep tests, within the theory of linear viscoelasticity, and test results are mathematically expressed in the form of a Prony series, as described in Chapter 3. In addition, the cohesive zone model was used to simulate the fracture process of asphalt surface layers due to thermal-mechanical loading, which was also described in Chapter 3.

4.3. Layer Properties

Table 4.1 presents the material properties of individual layers for each pavement structure (ST1, ST2, and ST3). The underlying layers of the pavement structures (i.e., PCC, existing AC, base, and subgrade) were modeled as isotropic thermo-elastic, while the isotropic thermo-viscoelastic response with cohesive zone fracture was considered to describe the behavior of the asphalt concrete surface layer. For simplicity, a Poisson's ratio of 0.30 was assumed for all layers. The coefficients of thermal expansion of asphalt mixtures (asphalt overlay and existing old asphalt) and PCC slab were assumed as $2.5 * 10^{-5}/^{o}C$ and $9.9 * 10^{-5}/^{o}C$, respectively. The interface between each layer was assumed to be fully bonded.

Table 4.1 Material properties of each layer

Linear Elastic Properties			
Layer	*E* (MPa)		*v*
PCC Slab	26,200		0.30
Existing Asphalt	2,413.2		
Base	151.68		
Subgrade	43		
Linear Viscoelastic Prony Series Parameters (with *v* = 0.30 and at -10°C of θ^R)			
Asphalt Overlay	*i*	ρ_i (sec)	E_i (MPa)
	1	0.00001	819.3
	2	0.0001	1,034.4
	3	0.001	1,817.1
	4	0.01	2,812.7
	5	0.1	4,195.4
	6	1.0	5,660.2
	7	10	6,614.8
	8	100	6,291.0
	9	1,000	4,634.1
	10	10,000	2,601.5
	11	100,000	2,273.9
	∞	-	324.8
WLF Model Parameters (at -10°C of θ^R)			
Asphalt Overlay	C_1 = 20.72, C_2 = 90.74		
Cohesive Zone Fracture Properties			
Asphalt Overlay	Temperature	T_{max} (Pa)	Γ_c (J/m^2)
	0	$3.2 * 10^5$	1,076
	-10	$3.2 * 10^5$	450
	-20	$3.2 * 10^5$	330
	-30	$3.2 * 10^5$	210
Coefficient of Thermal Expansion (/°C)			
Asphalt Overlay	$2.5 * 10^{-5}$		
Existing Asphalt	$2.5 * 10^{-5}$		
PCC Slab	$9.9 * 10^{-5}$		

4.4. Loading

This subsection presents two loads (thermal and mechanical) to which the pavement structure was subjected. Thermal loading was applied to the entire pavement structure based on the spatial and temporal temperature profile using the user-defined temperature subroutine, UTEMP, and mechanical loading due to truck tires was applied on the asphalt surface.

4.4.1. Thermal Loading

As mentioned earlier, thermal cracks in pavements often occur in a single, critical cooling event. Thus, prior to performing the thermal cracking simulation, the critical cooling events need to be researched from historical climate data. Temperature gradients with respect to the pavement depth for each pavement structure were estimated from the pavement surface temperature using an enhanced integrated climate model (EICM) developed by AASHTO.

In order to select the critical cooling event for the past 10 years, the historical temperature data in the city of Lincoln, Nebraska, were researched. According to the temperature data from 1995 to 2005, it was found that the coldest temperature occurred in January of 2005. In that month, the air temperature dropped down to -22.1^{o}C and the average daily temperature change was -6^{o}C. Using the EICM, the critical temperature gradients and cooling cycles were estimated for the three different pavement structures (ST1, ST2, and ST3), as shown in figure 4.3. As illustrated in the figure, although the surface temperature of each pavement structure is equal, it varies with pavement depth depending on the underlying layers. In addition, the temperature variation with respect to time is significant at the surface but it diminishes as the pavement depth increases.

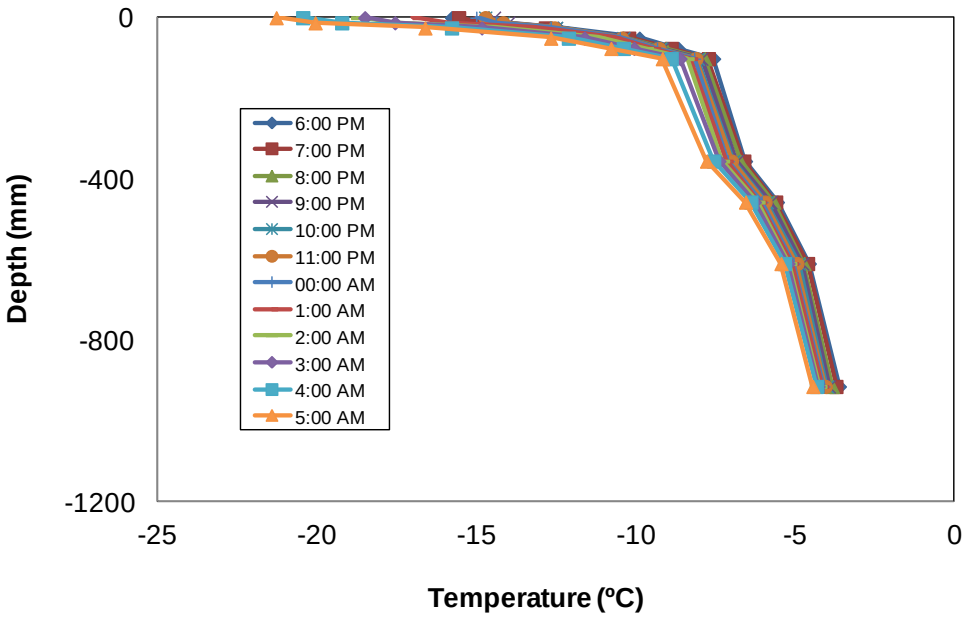

(a) pavement ST1

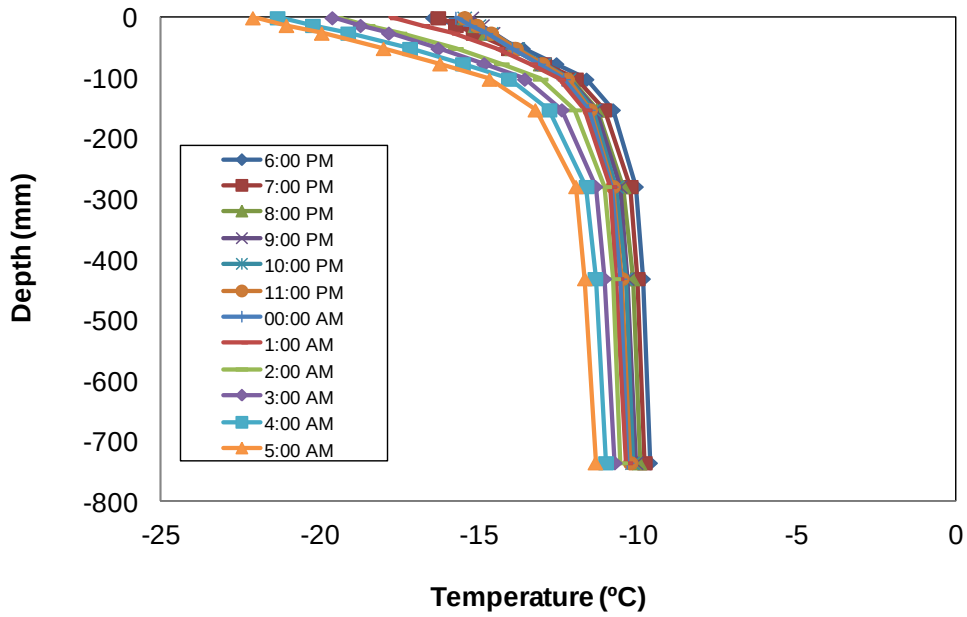

(b) pavement ST2

Figure 4.3 Temporal and spatial temperature variations

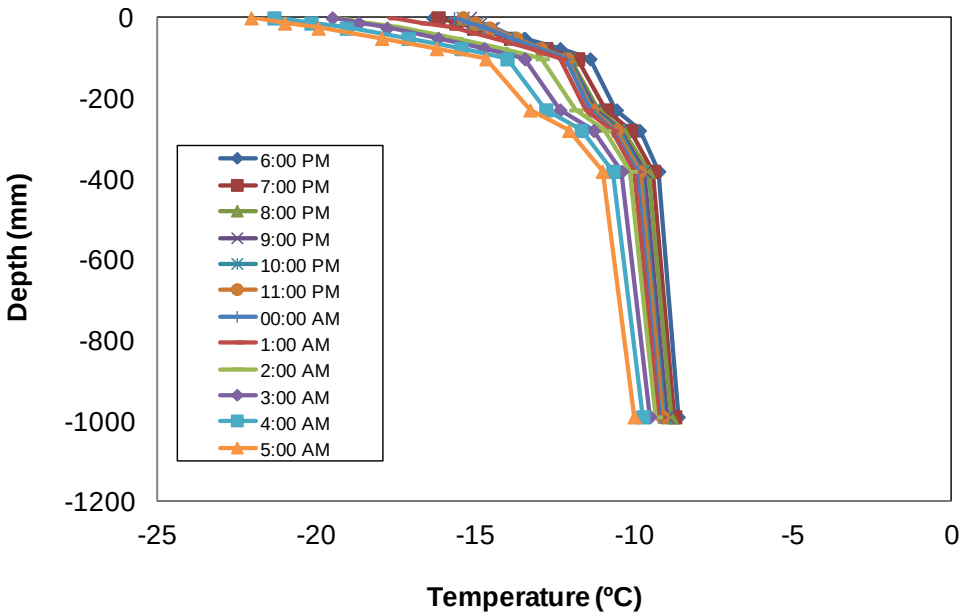

(c) pavement ST3

Figure 4.3 Temporal and spatial temperature variations cont'd

Based on the temperature profiles presented in figure 4.3, the time- and depth-dependent temperature profiles were implemented into the model through the user-defined temperature module (UTEMP). As observed in the figure, temperature decreases exponentially as depth increases. Thus, the temperature with depth ($T(h)$) was presented as an exponential function and each coefficient was related with time in the form of a fourth-order polynomial, as expressed by the following set of equations:

$$\begin{aligned} T(h) &= A_0(t) + A_1(t)\left[1 - \exp\left(-A_2(t)\cdot h\right)\right] \\ A_0(t) &= A_{00} + A_{01}t + A_{02}t^2 + A_{03}t^3 + A_{04}t^4 \\ A_1(t) &= A_{10} + A_{11}t + A_{12}t^2 + A_{13}t^3 + A_{14}t^4 \\ A_2(t) &= A_{20} + A_{21}t + A_{22}t^2 + A_{23}t^3 + A_{24}t^4 \end{aligned} \tag{4.7}$$

A least-square type error minimization was carried out to obtain the best-fitting model coefficients, which resulted in a coefficient matrix (3 by 5). A total of 15 coefficients would be sufficient to model the spatial and temporal temperature variations during the critical cooling event. For purposes of verification, figure 4.4 compares predicted temperatures from UTEMP to the actual temperature data of ST1 pavement as an example. It clearly demonstrates that the temperature approximation by the user subroutine can be successfully used to prescribe the temperature field in the finite element simulations.

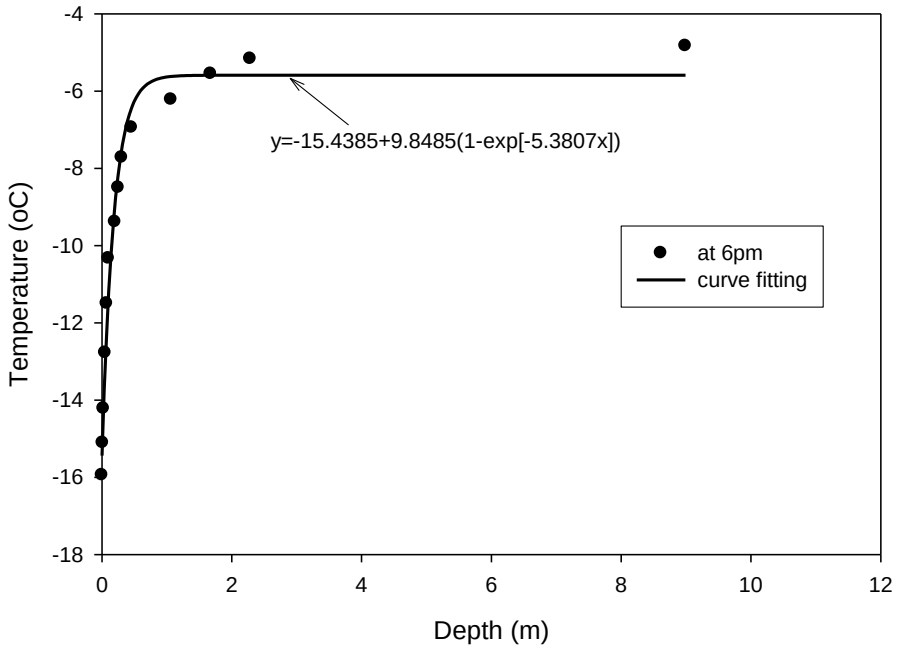

(a) spatial temperature variation at a specific time

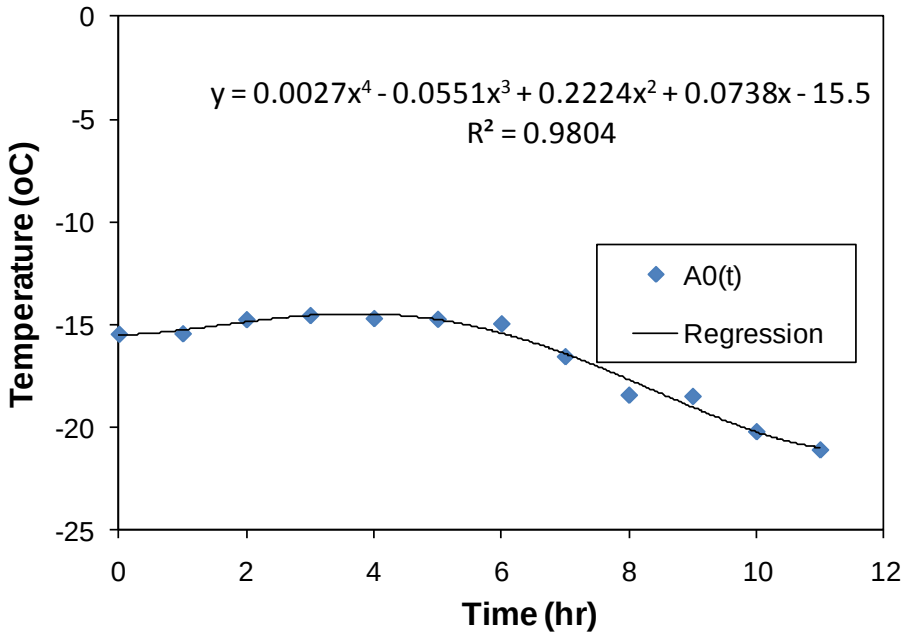

(b) temporal temperature variation at a specific location

Figure 4.4 Verification of UTEMP to prescribe temperature field in the simulations

4.4.2. Mechanical Loading

Figure 4.5 illustrates the loading configuration of the Class 9 truck used in this study. Although the truck loading consisted of a front steering axle and two tandem axles with dual tires, to reduce computational time in the analysis, only the two tandem axles with dual tires were selected through use of the trapezoidal loading sequence, shown in figure 4.6. A 15.4 m Class 9 truck trailer traveling at 80 km/h takes 0.692 seconds to pass over a fixed point on the pavement. Therefore, the first truck passes the fixed point for 0.692 seconds and, after 192 seconds, a second truck passes through the same point. The passage of 450 trucks was simulated based on the information of the daily maximum amount of truck passes reported by the Nebraska Department of Road (NDOR).

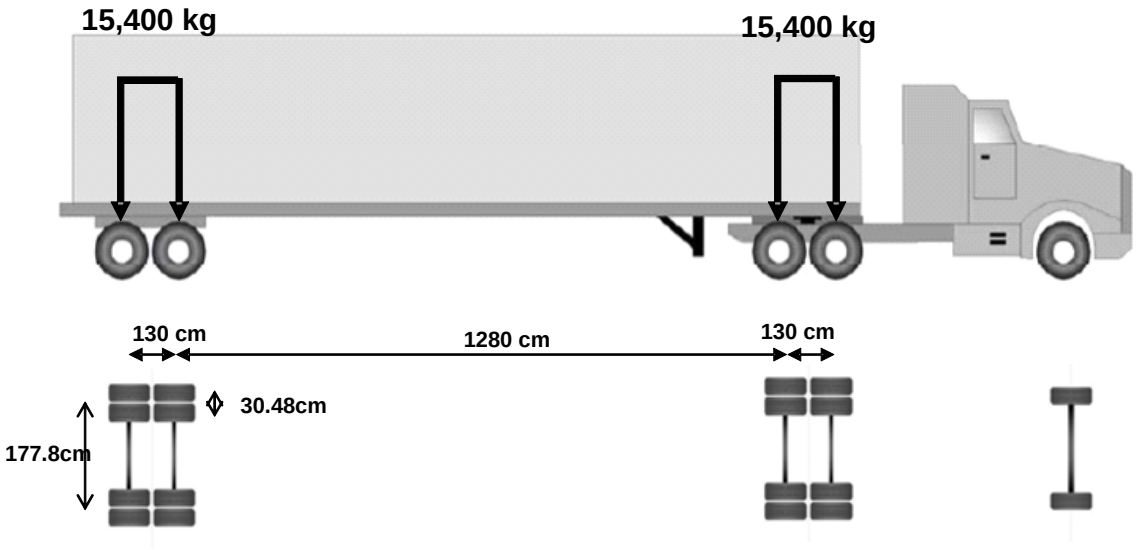

Figure 4.5 Loading and axle configuration of the Class 9 truck used for this study

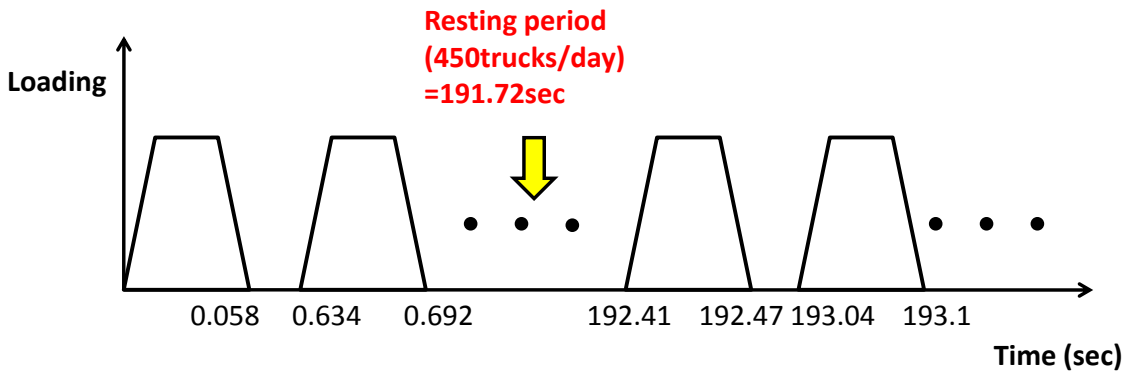

Figure 4.6 Truck loading sequence applied to the pavement simulations

4.5. Simulation Results

This subsection presents the numerical simulation results of the pavement responses due to thermal loading only and when the mechanical loading was incorporated with the thermal loading. Among many mechanical pavement responses, the tensile stresses at the surface and at the bottom of the asphalt overlay, and the crack opening displacement through the depth of the asphalt overlay, were examined during the 12 hr cooling event with and without truck loading. This was because the tensile stresses and the crack opening displacements of the asphalt overlay are significant indicators to predict cracking and performance behavior of asphaltic pavements at low-temperature conditions.

Parametric analyses were then conducted by varying pavement geometries and material properties to better understand the mechanical sensitivity of design variables on the overall responses and performance characteristics of pavement structures. This understanding can lead to the selection of paving materials in a more appropriate manner and to the provision of scientific insights into the more optimized pavement design at low-temperature conditions.

4.5.1. ST1 Simulation with Thermal Loading Only

Figure 4.7 presents horizontal stresses on the surface and at the bottom of the ST1 asphalt overlay during the 12 hr cooling event. It shows that the asphalt overlay experienced compression at the top of the layer until 12:00 a.m., but it was then subjected to increasing tension, while the bottom of the asphalt overlay was always in tensile stress. After around 1:30 a.m., the magnitude of the tensile stress on the surface became greater than the tensile stress at the bottom of the layer. At the last stage of the cooling cycle, the tensile stress reached the cohesive zone strength (i.e., critical traction) of 3.2 MPa, which implies the onset of softening to top-down cracking. However, the top-down cracking did not progress further to complete failure, as the solid line shown in figure 4.7 did not drop to the zero stress.

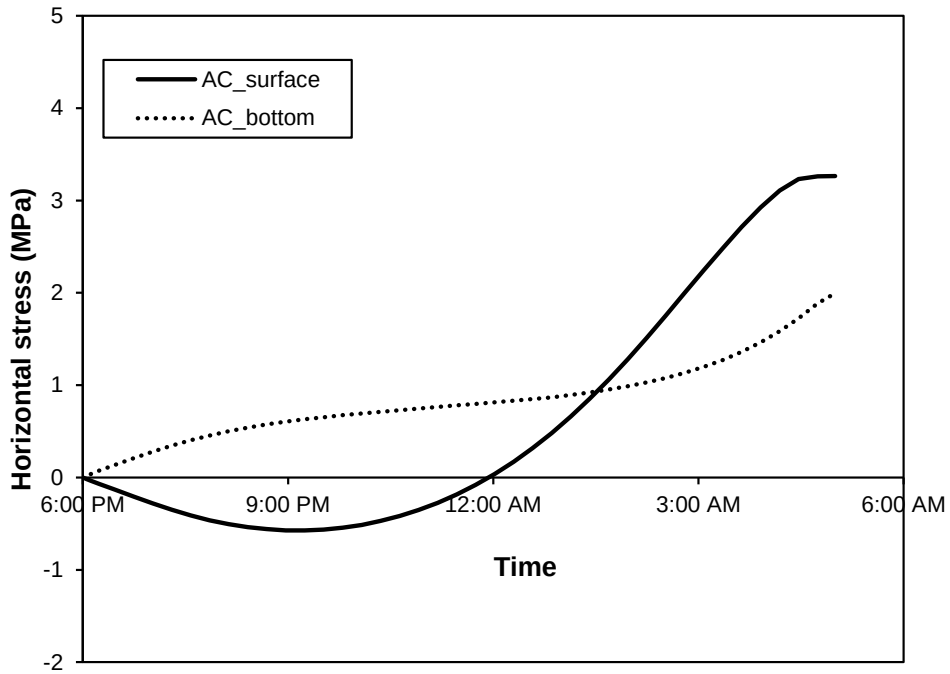

Figure 4.7 Horizontal stresses at the surface and at the bottom of the ST1 asphalt overlay

Based on the simulation results with given default pavement geometry and layer properties, parametric analyses were attempted by varying asphalt overlay thicknesses and/or material properties of the asphalt overlay. When the overlay thickness changed, a new temperature profile was necessary for the simulation because of the overall pavement geometry change. Figure 4.8 presents a new set of temperature profiles over the pavement depth for the 12 hr cooling cycle, when the asphalt overlay thickness was reduced to 50.8 mm, which is half of the default thickness of 101.6 mm asphalt overlay.

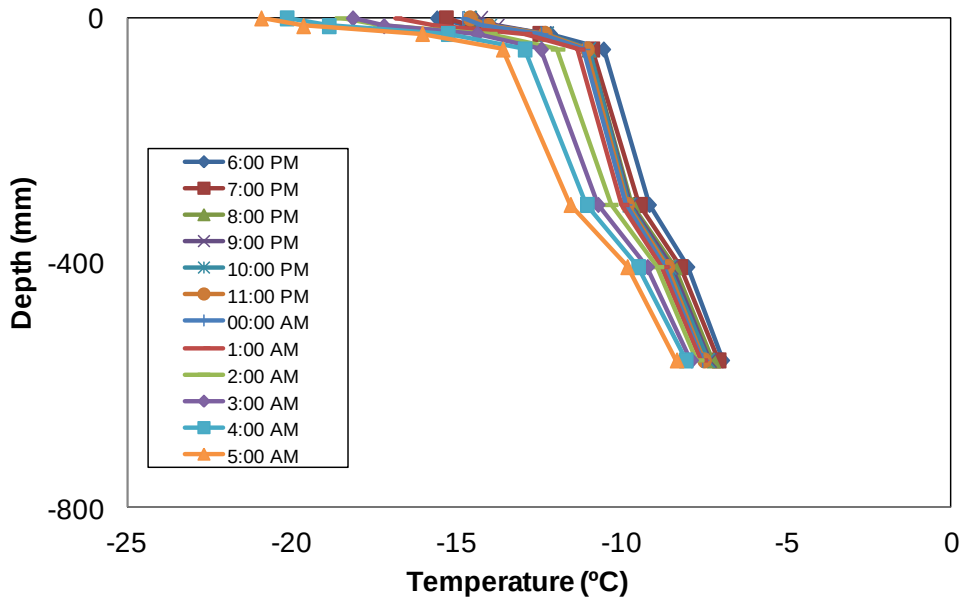

Figure 4.8 Temperature profiles of a 50.8 mm thick asphalt overlay of ST1

Figure 4.9 compares temperature variations over the 12 hr cooling cycle at the two significant locations (surface and bottom of the overlay) when the two different overlay thicknesses were used. As expected and seen in the figure, the temperature variation between the two structures is identical at the layer surface, while the lower temperatures and higher variations

were observed at the bottom of the asphalt surface layer from the 50.8 mm case. This is because of the higher insulation of the thicker layer.

Due to the lower temperature and greater temperature susceptibility of the thinner structure, the 50.8 mm pavement eventually failed, as illustrated in figure 4.10, during the cooling event. More specifically, the pavement abruptly failed by separation triggered from both directions at the maximum cooling rate, which is around 4:00 - 5:00 a.m.

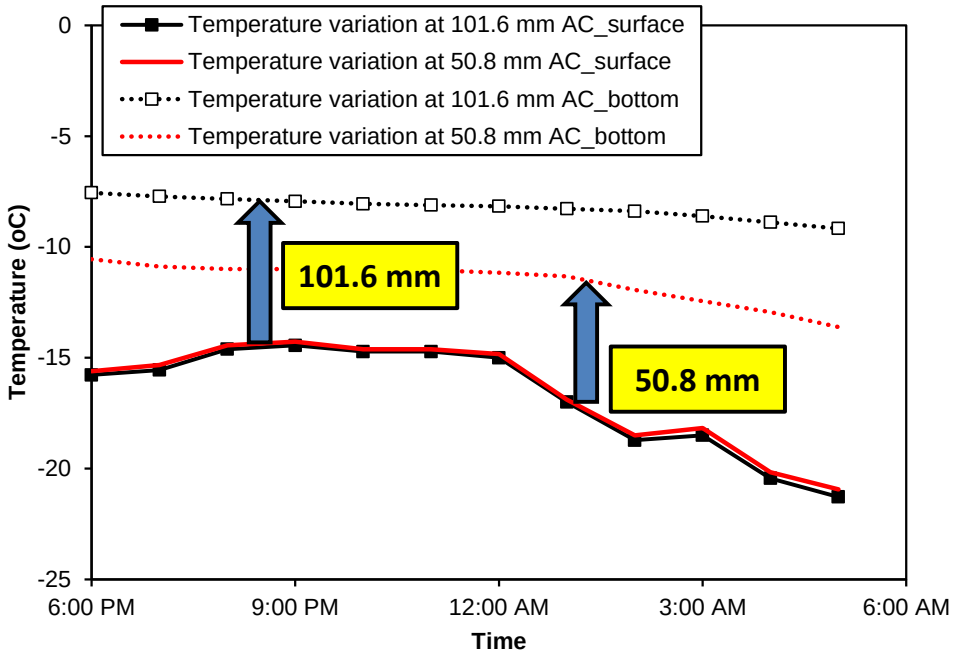

Figure 4.9 Temperature variations: 101.6 mm vs. 50.8 mm overlay thickness

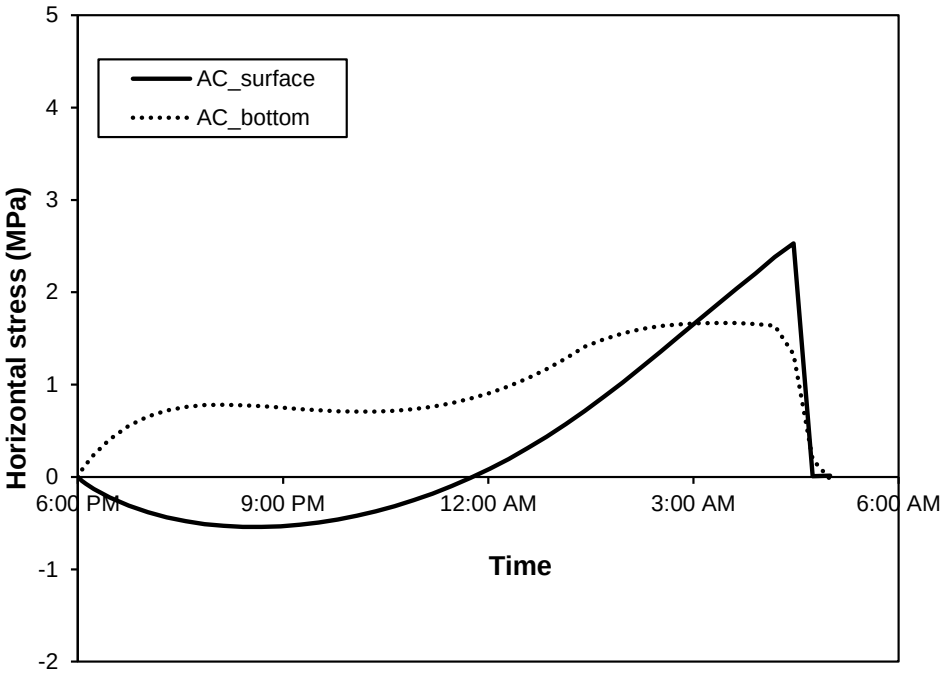

Figure 4.10 Horizontal stresses at the surface and at the bottom of ST1 asphalt overlay with reduced thickness: 50.8 mm

In an attempt to investigate the effects of engineered properties of paving materials on performance behavior, two other simulations were conducted by varying two different categories of layer properties: the coefficient of thermal expansion and the fracture property of the asphalt overlay. According to a study by Mamlouk et al. (2005), the coefficient of thermal expansion of asphalt concrete mixtures typically ranges from $1.1 * 10^{-5}/^{o}C$ to $3.71 * 10^{-5}/^{o}C$. Thus, in this study, the lowest bound value (i.e., $1.1 * 10^{-5}/^{o}C$) was tried and compared to the case with the default value (i.e., $2.5 * 10^{-5}/^{o}C$) to examine to what degree cracking resistance of the pavement can be improved due to the engineered material property. Regarding the effects of fracture property, a 30% increase of the default cohesive zone strength (T_{max}) was used. For all the cases, the simulation result in figure 4.10 was compared as a reference case. Figures 4.11(a) and (b) present the simulation results. As shown in the figures, pavements with engineered properties could last during the cooling cycle without fracture. The simulation results shown in figure

4.11(a) indicate that the lower coefficient of thermal expansion could significantly reduce the tensile stress at the asphalt surface, although it did not change tensile stresses at the bottom of the asphalt overlay. When the asphalt overlay was more crack resistant with the increased cohesive zone strength, as illustrated in figure 4.11(b), the pavement did not show thermal cracking, since the resulting tensile stress was lower than the critical stress state causing material separation. From the simulation results shown herein, it can be concluded that the engineered paving materials can significantly contribute to the reduction of pavement thickness, which could lead to much more economic and optimized pavement structural design.

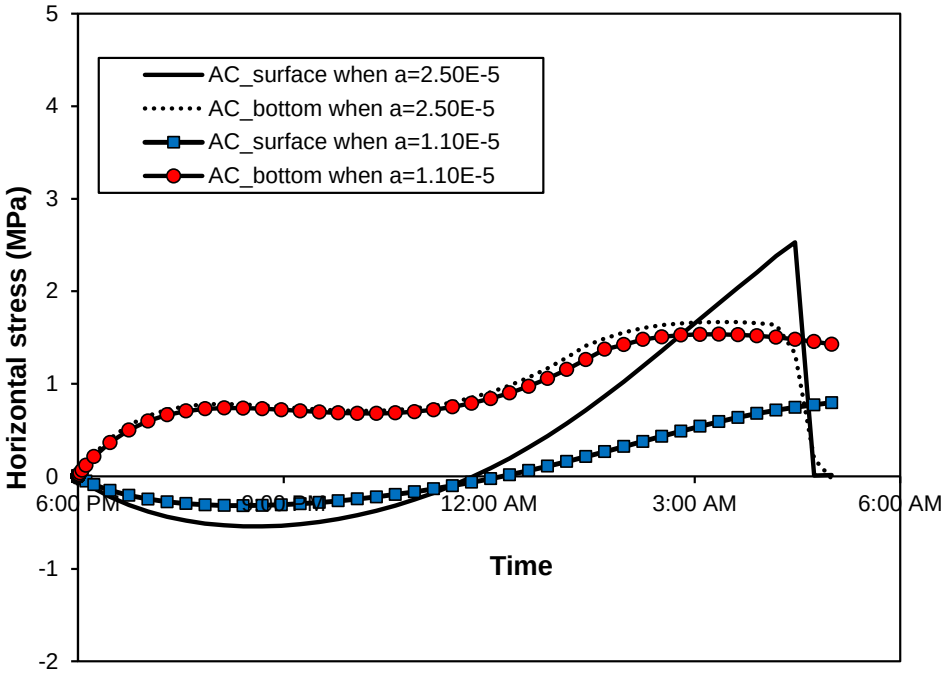

(a) $\alpha = 2.5 * 10^{-5}/^{o}C$ vs. $1.1 * 10^{-5}/^{o}C$

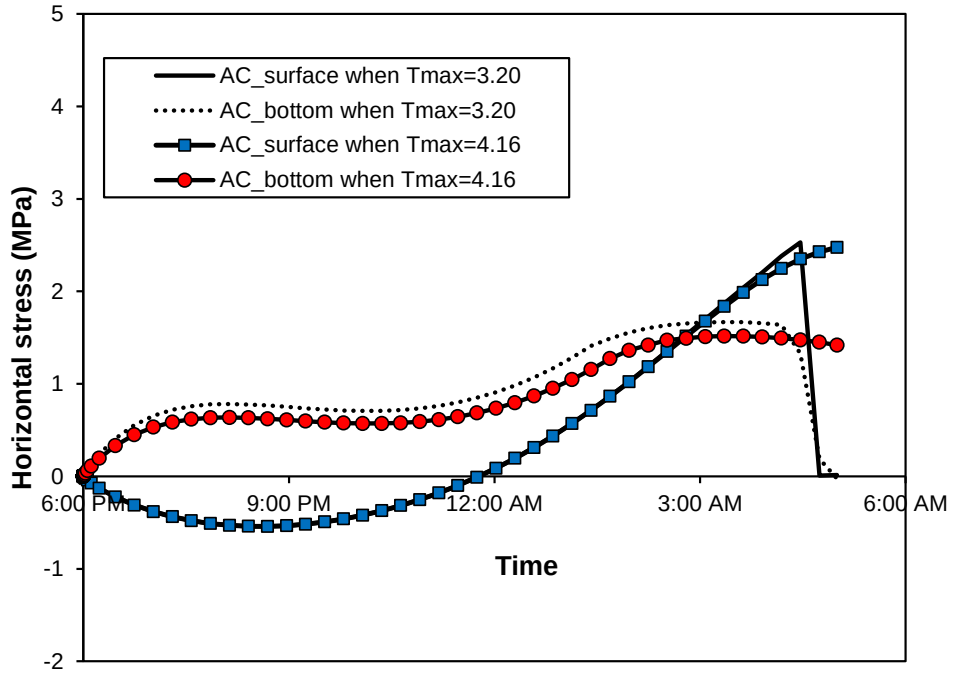

(b) T_{max} = 3.2 MPa vs. T_{max} = 4.16 MPa

Figure 4.11 Simulation results with engineered material properties

4.5.2. ST2 Simulation with Thermal Loading Only

Figure 4.12 presents horizontal stresses on the surface and at the bottom of the ST2 asphalt overlay during the 12 hr cooling event. Similar to the results of the ST1 structure, the asphalt overlay experienced compression at the top of the layer for about six hours, and then it was subjected to increasing tension until it met the softening threshold. The horizontal stress at the bottom of the asphalt overlay is, however, mostly under a tensile state. At around 2:00 a.m., the magnitude of tensile stress on the overlay surface reached the cohesive strength (3.2 MPa), which triggered the progressive material softening, followed by fracture. Top-down cracking occurred, as the figure shows zero traction on the surface of asphalt overlay at the end of the simulation.

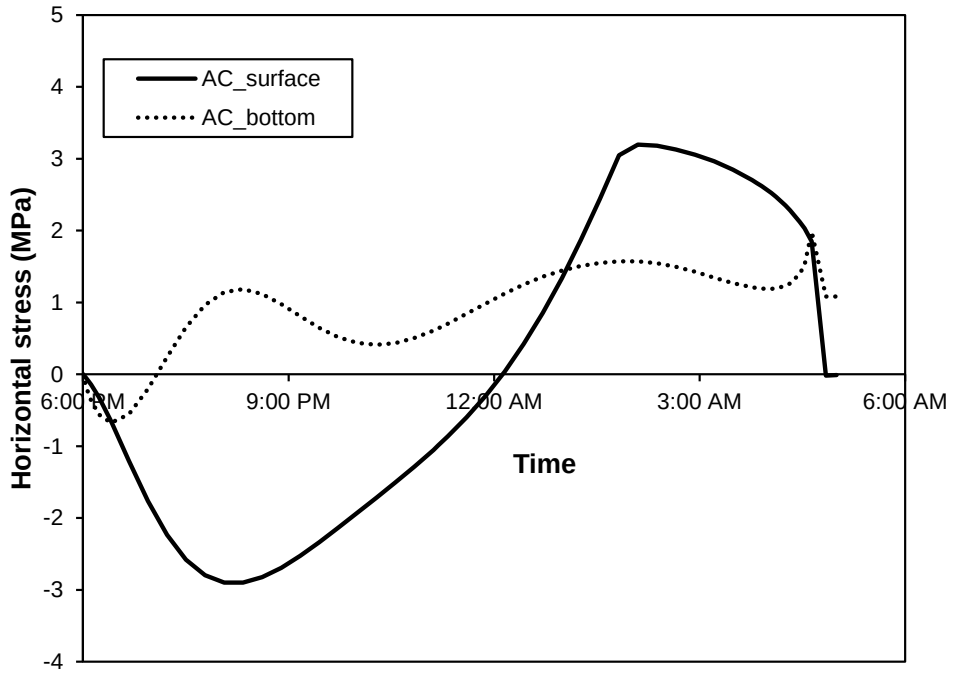

Figure 4.12 Horizontal stresses at the surface and at the bottom of ST2 asphalt overlay

Since the top-down thermal cracking was expected in the ST2 pavement when it was designed with the default values of layer thickness and measured values of material properties, some design alternatives could be considered to improve pavement performance at low-temperature conditions. Better pavement performance can be achieved by either increasing the overlay thickness or replacing the current materials with engineered ones. Figure 4.13 presents simulation results when the asphalt overlay material has been modified to represent lower temperature susceptibility (i.e., a lower value of the coefficient of thermal expansion) or greater fracture resistance with an improved cohesive strength by 30%. In both cases, the ST2 pavement did not fail due to the thermal cracking, even though it experienced a softening process. Clearly, engineered paving materials allow the pavement structure to perform better by being able to sustain the damage and avoid failure.

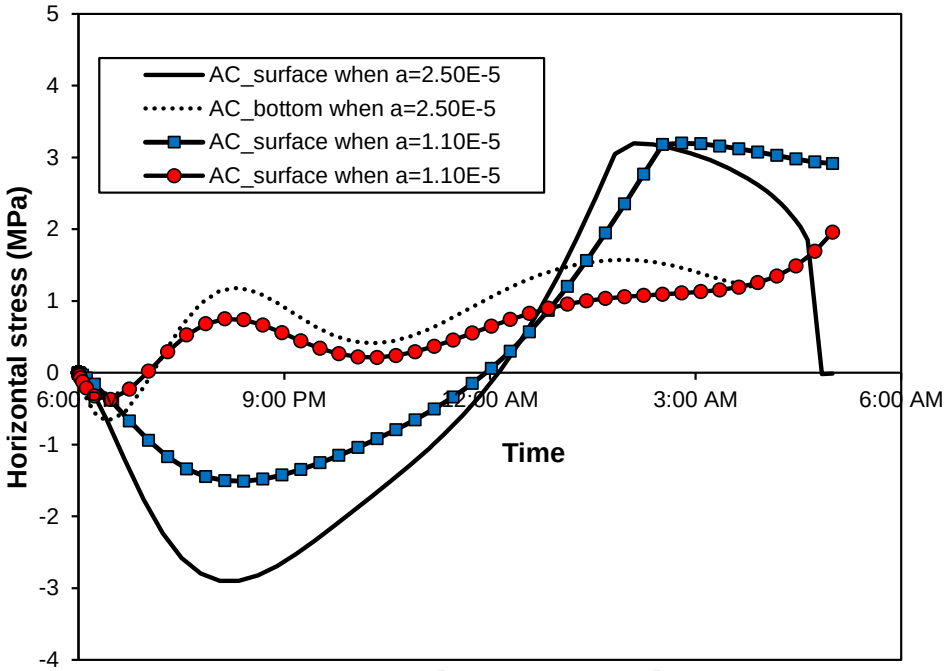

(a) $\alpha = 2.5 * 10^{-5}/^{o}C$ vs. $1.1 * 10^{-5}/^{o}C$

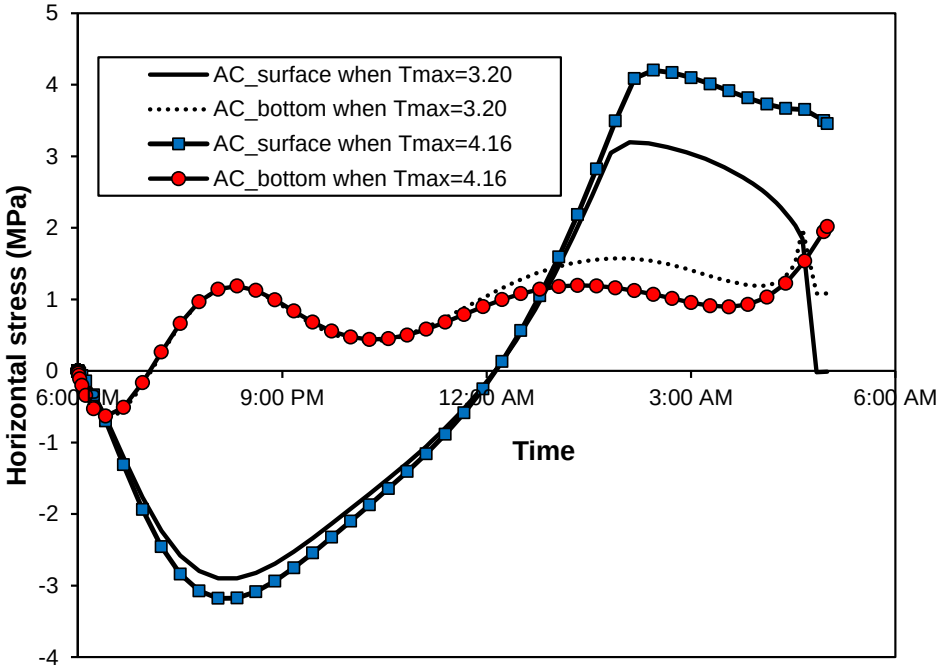

(b) T_{max} = 3.2 MPa vs. T_{max} = 4.16 MPa

Figure 4.13 Simulation results with engineered material properties (ST2)

4.5.3. ST3 Simulation with Thermal Loading Only

Simulation results of horizontal stresses on the surface and at the bottom of the ST3 pavement are presented in figure 4.14. In comparison with the results of the ST2 pavement, ST3 sustained no cracking through the 12 hr cooling cycle. At the top of the layer, the asphalt overlay was in compression for six hours, and then was subjected to increasing tension, while the horizontal stress at the bottom of the layer was completely in tension. The overlay surface met the softening threshold at around 2:00 a.m., which implies the onset of top-down damage (material softening). However, thermal cracking did not occur as the figure shows residual resistance of the layer at the end of the cooling cycle.

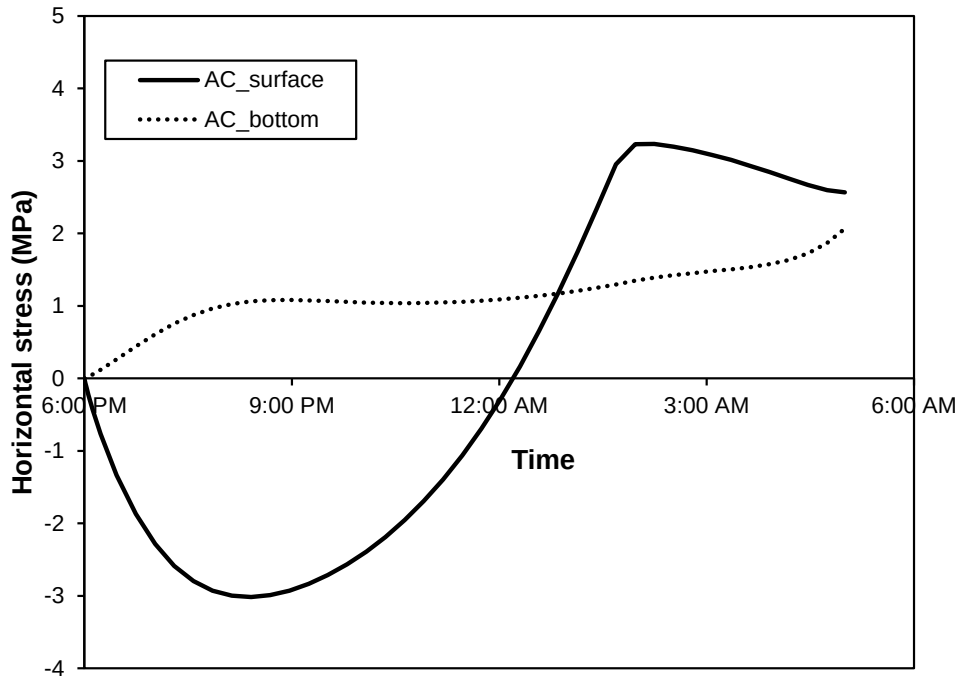

Figure 4.14 Horizontal stresses at the surface and at the bottom of ST3 asphalt overlay

Based on the simulation results from the default pavement geometry and the layer properties of ST3, several additional simulations were attempted. Figure 4.15 presents a new set of temperature profiles over the pavement depth to conduct model simulations with the reduced thickness of asphalt overlay to 50.8 mm, and figure 4.16 shows simulation results plotting horizontal stresses at the two critical locations (top and bottom of the asphalt overlay) over time.

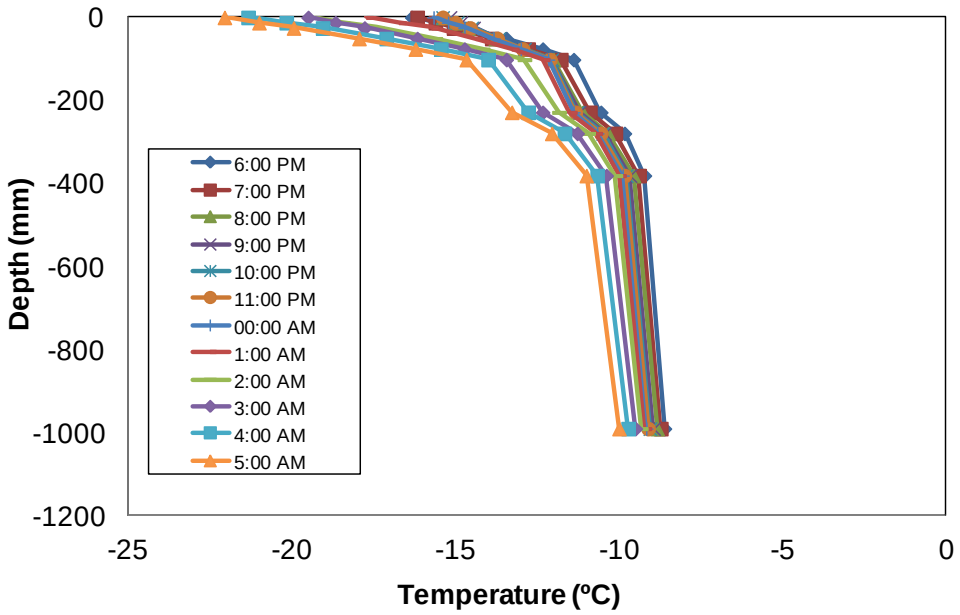

Figure 4.15 Temperature profiles of 50.8 mm thick asphalt overlay of ST3

As presented in figure 4.16, the tensile stresses both at the surface and at the bottom of the asphalt overlay reached the critical traction around 8 hrs into the cooling cycle and eventually dropped down to zero, implying that the pavement layer fully cracked due to the thermal loading. This was an expected result since the thinner overlay presents higher gradients of thermal strain, which corresponds to greater thermal cracking susceptibility than the thicker layer.

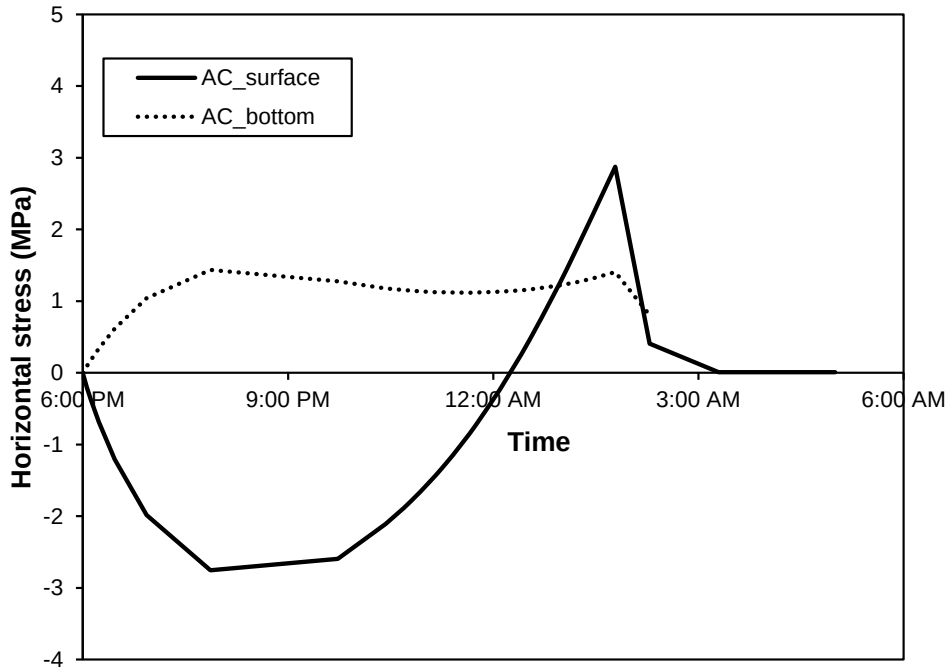

Figure 4.16 Horizontal stresses at the surface and at the bottom of the ST3 asphalt overlay with reduced thickness: 50.8 mm

Figure 4.17 illustrates the simulation results with improved overlay properties: 4.17(a) using the smaller coefficient of thermal expansion ($1.1 * 10^{-5}/^{o}C$) and 4.17(b) using the increased fracture resistance by 30%. As seen earlier from other structures and this example, the improved layer properties obviously contributed to the better pavement performance. For both cases, thermal cracking did not occur through the cooling cycle. Figure 4.17(a) presents the effect of thermal expansion potential of asphalt overlay in that the lower value of thermal expansion can significantly reduce the tensile stress at the surface of the asphalt layer. With greater resistance to fracture, the asphalt overlay could sustain the thermal loading without physical cracking, as demonstrated in figure 4.17(b). Using superior materials can vastly reduce pavement thickness for the similar level of performance.

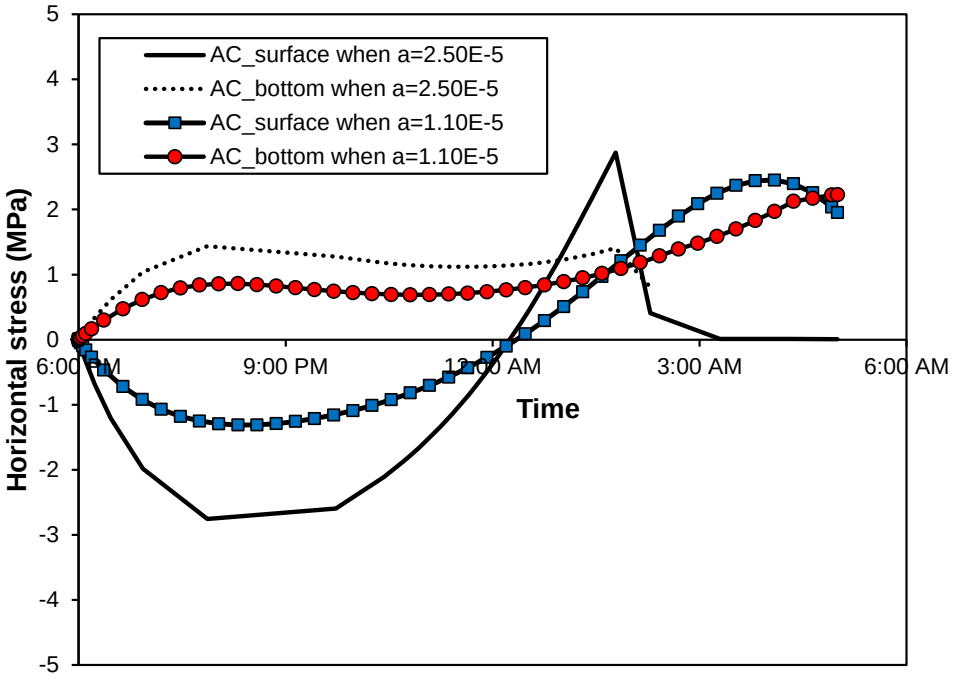

(a) $\alpha = 2.5 * 10^{-5}/^{o}C$ vs. $1.1 * 10^{-5}/^{o}C$

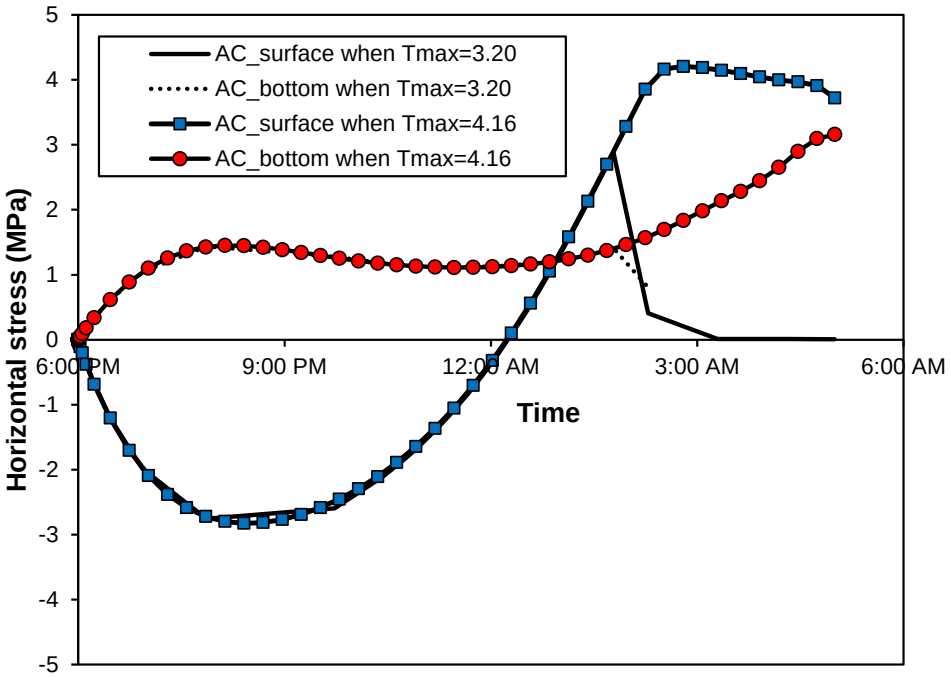

(b) T_{max} = 3.2 MPa vs. T_{max} = 4.16 MPa

Figure 4.17 Simulation results with engineered material properties (ST3)

Another set of simulations was also attempted by applying poorer materials to the reference pavement geometry of 101.6 mm thick asphalt overlay. Based on the study by Mamlouk et al. (2005), who presented the typical range of α value from $1.1 * 10^{-5}/^{o}C$ to $3.71 * 10^{-5}/^{o}C$, the highest bound value (i.e., $3.71 * 10^{-5}/^{o}C$) was tried and compared to the case with the default value (i.e., $2.5 * 10^{-5}/^{o}C$) to examine how much the cracking resistance of the pavement would be reduced. Regarding the effects of fracture property, a 30% decrease of the default cohesive zone strength was used. As illustrated in figure 4.18, the ST3 pavement fully cracked in both cases. Inferior materials clearly induced more damage and premature failure of the structure. Simulation results herein and earlier indicate that the performance-based pavement design can be achieved by mechanistic analyses of the pavement structure based on the fundamental properties of the layer materials.

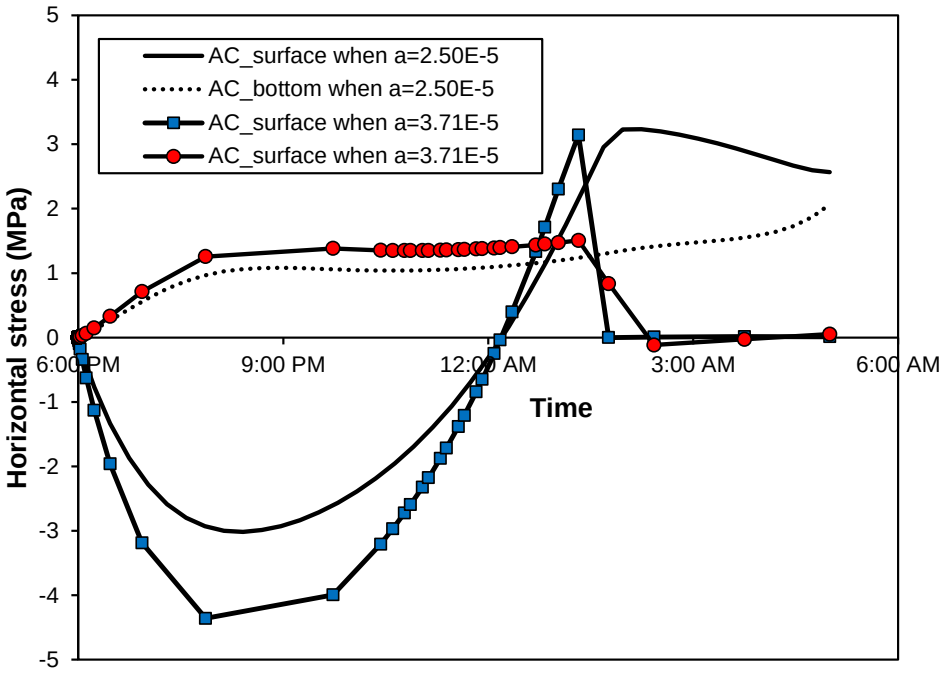

(a) $\alpha = 2.5 * 10^{-5}/^{o}C$ vs. $3.71 * 10^{-5}/^{o}C$

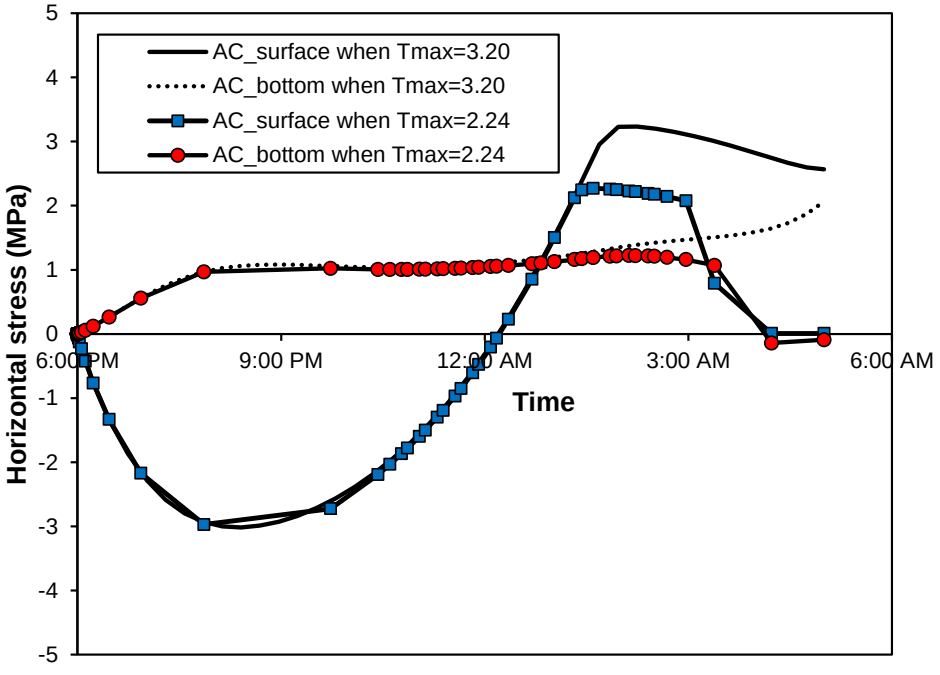

(b) T_{max} = 3.2 MPa vs. T_{max} = 2.24 MPa

Figure 4.18 Simulation results with degraded material properties (ST3)

4.5.4. ST1 Simulation with Thermal and Mechanical Loading

Although it has been known that pavement cracks often occur in a single, critical cooling event at low-temperature conditions, the effects of heavy vehicles on pavement damage also need to be investigated since the pavement, in reality, is subjected to the truck loads and low temperatures simultaneously. To that end, thermo-mechanical model simulations were also conducted in this research. For the simulation, the ST1 pavement with its default pavement geometry and material properties was selected, and the Class 9 truck trailer illustrated in figure 4.5 was applied to the pavement to represent vehicles traveling at 80 km/h for a total of 450 passages. To represent critical traffic loading conditions, the truck tire loading was placed right above the cohesive zone elements.

As in other simulations with thermal loading only, the horizontal stresses and cohesive zone opening displacements over the depth of asphalt overlay were monitored. Simulation results were then compared to the results from the reference case in order to examine the effects of mechanical loading on the pavement performance at low-temperature conditions. Figure 4.19 presents the model simulation results plotting the cohesive zone opening displacements within the asphalt overlay, at the end of the cooling cycle (i.e., 5:00 a.m.) and truck passing (i.e., 450 passes). As shown in the figure, no huge discrepancy was observed in the cohesive zone opening displacement between the two cases. This implies that the mechanical truck loading does not affect pavement damage and failure significantly at low-temperature conditions, which subsequently infers that the truck loading could be ignored for the structural design of pavements associated with low temperatures.

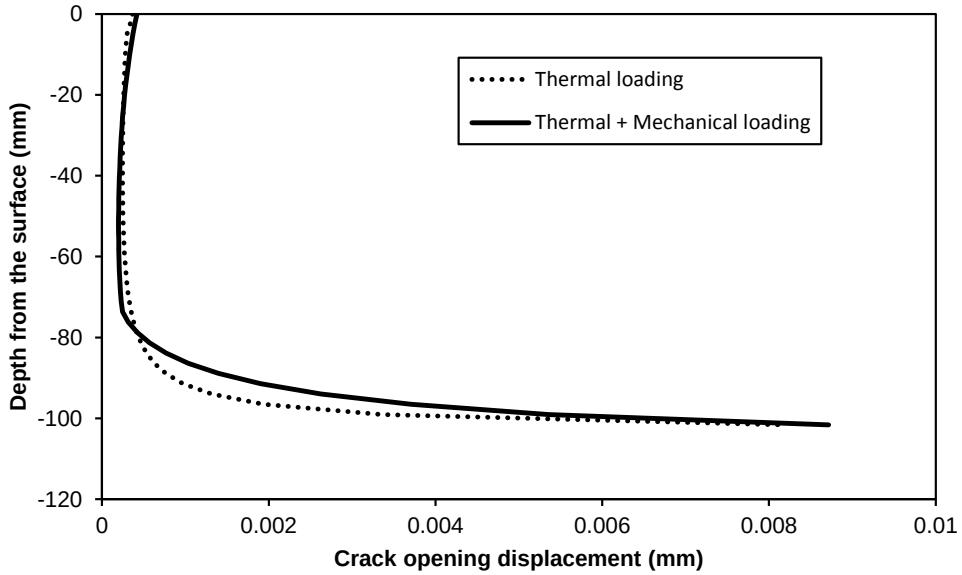

Figure 4.19 Thermo-mechanical pavement response

Chapter 5 Summary and Conclusions

This research project investigated the performance and damage characteristics of Nebraska roadways at low-temperature conditions. To meet the research objective, laboratory tests were incorporated with mechanistic numerical modeling. Three of the most common pavement structures in Nebraska were selected and modeled considering local environmental conditions and pavement materials, with and without truck loading. Cracking of asphalt overlay was predicted and analyzed by conducting finite element simulations incorporated with a user-defined temperature subroutine and cohesive zone fracture. Parametric analyses were also conducted by varying pavement geometries and material properties, which could lead to helping pavement designers understand the mechanical sensitivity of design variables on the overall responses and performance characteristics of pavement structures. This better understanding is expected to provide NDOR engineers with more scientific insights for the selection of paving materials in a more appropriate way and to advance the current structural pavement design practices. Based on the test and simulation results, the following conclusions were drawn.

5.1. Conclusions

- Two-dimensional finite element simulation was successfully conducted for predicting the thermo-mechanical performance of typical asphaltic pavement structures in Nebraska. The finite element modeling was integrated with experimental tests to investigate the fracture process (initiation and propagation of cracks) of asphaltic pavements due to thermal and/or mechanical loading.
- Nonlinear temperature gradients, which are time dependent and spatially variant, were effectively implemented into the finite element modeling by using the national climate data, the enhanced integrated climate model (EICM), and the user-defined temperature

module (UTEMP), which was developed for this research. Model simulations were conducted by projecting the nonlinear temperature data into the finite element mesh for the coldest 12 hr cooling cycle (6:00 p.m. to 5:00 a.m.) in hourly time steps.

- All pavement structures examined in this project presented sensitive mechanical responses due to the thermal loading. In addition, pavement responses were significantly affected by variation of pavement geometry and layer material properties, such as the coefficient of thermal expansion and fracture characteristics. Engineered paving materials, such as the one with 30% improved fracture resistance, could reduce surface layer thickness by 50% to meet the similar low-temperature performance.
- The effects of heavy vehicles on the pavement damage at low-temperature conditions were investigated by applying thermal loading and mechanical truck loading simultaneously. This thermo-mechanical finite element simulation demonstrated that no huge discrepancy in the cohesive zone opening displacement occurred compared to the case with thermal loading only. This implies that the mechanical truck loading does not affect pavement damage and failure significantly at low-temperature conditions, which subsequently implied that the truck loading could be ignored for the structural design of pavements associated with low temperatures.
- The mechanistic approach based on fundamental theories and material characteristics seems very reasonable and useful to better aid in the selection of paving materials and to enable performance-based pavement design. Nevertheless, field validation is necessary to prove the benefits and accuracy of the finite element pavement modeling. Therefore, it is recommended to continue this effort for advancing the current pavement design concept, which will be more and more mechanistic in the future.

Chapter 6 NDOR Implementation Plan

NDOR plans on expanding the SCB test to production on actual projects during construction to gather their SCB strengths and correlating them to field performance in an effort to guide potential future designs for thickness, and support same and better low temperature crack resistant leveling courses, base layers and surface layers. This will support the thin lift strategies that are becoming so important and vital to Nebraska's and the nation's resurfacing strategies.

References

AASHTO TP 62-07. 2008. "Determining dynamic modulus of hot-mix asphalt concrete mixtures." *Standard Specifications for Transportation and Methods of Sampling and Testing, 28th Edition, and Provisional Standards*. America Association of State Transportation and Highway Engineering.

ABAQUS. 2008. "Version 6.8." Hibbt, Karlsson, and Sorenson, Inc.: Pawtucket, Rhode Island.

Aragão, F. T. S. 2011. "Computational microstructure modeling of asphalt mixtures subjected to rate-dependent fracture." Ph.D. Dissertation, University of Nebraska, Lincoln.

Bazant, Z. P. and J. Planas. 1998. *Fracture and size effect in concrete and other quasibrittle materials*. Boca Raton, FL: CRC Press LLC.

Dave, E. V., S. H. Song, W. G. Buttlar, and G. H. Paulino. 2007. " Reflective and thermal cracking modeling of asphalt concrete*." Proceedings of the Advanced Characterization of Pavement and Soil Engineering Materials*, Athens, Greece, 1241-1252

Dave, E. V. and W. G. Buttlar. 2010. "Thermal reflective cracking of asphalt concrete overlays." *International Journal of Pavement Engineering* 11, no. 6: 477-488.

Duan, K., X. Hu, and F. H. Wittmann. 2006. "Scaling of quasi-brittle fracture: boundary and size effect." *Mechanics of Materials* 38: 128-141.

Espinosa, H. D. and P. D. Zavattieri. 2003. "A grain level model for the study of failure initiation and evolution in polycrystalline brittle materials, part I: theory and numerical implementation." *Mechanics of Materials* 35: 333-364.

Geubelle, P. and J. Baylor. 1998. "Impact-induced delamination of laminated composites: a 2D simulation." *Composites Part B – Engineering* 29, no. 5: 589-602.

Hoare, T. R. and S. Hesp. 2000. "Low-temperature fracture testing of asphalt binders: regular and modified systems." *Transportation Research Record* 1728: 36-42.

Kim, H., M. P. Wagoner, and W. G. Buttlar. 2008. "Simulation of fracture behavior in asphalt concrete using a heterogeneous cohesive zone discrete element model." *Journal of Materials in Civil Engineering* 20, no. 8: 552-563.

Kim, H. and W. G. Buttlar. 2009. "Finite element cohesive fracture modeling of airport pavements at low temperatures." *Cold Regions Science and Technology* 57: 123-130.

Lee, N. K., G. R. Morrison, and S. Hesp. 1995. "Low temperature fracture of poluethylene-modified asphalt binders and asphalt concrete mixes." *Journal of the Association of Asphalt Paving Technologists* 64: 534-574.

Li, X. and M. O. Marasteanu. 2004. "Evaluation of the low temperature fracture resistance of asphalt mixtures using the semi-circular bend test." *Journal of the Association of Asphalt Paving Technologists* 73: 401-426.

Li, X. and M. O. Marasteanu. 2010. "The fracture process zone in asphalt mixture at low temperature." *Engineering Fracture Mechanics* 77: 1175-1190.

Mamlouk, M. S., M. W. Witczak, K. E. Kaloush, and N. Hasan. 2005. "Determination of thermal properties of asphalt mixtures." *Journal of Testing and Evaluation* 33, no. 2: 1-9.

Marasteanu, M. O., S. T. Dai, J. F. Labuz, and X. Li. 2002. "Determining the low-temperature fracture toughness of asphalt mixtures." *Transportation Research Record* 1789: 191-199.

Marasteanu, M. O., A. Zofka, M. Turos, X. Li, R. Velasques, W. Buttlar, G. Paulino, A. Braham, E. Dave, J. Ojo, H. Bahia, C. Williams, J. Bausano, A. Gallistel, and L. McGraw. 2007. "Investigation of low temperature cracking in asphalt pavements: national pooled fund study 776." *Final Report No. MN/RC 2007-43*, Minnesota Department of Transportation.

Mobasher, B., M. S. Mamlouk, and H. M. Lin. 1997. "Evaluation of crack propagation properties of asphalt mixtures." *Journal of Transportation Engineering*, 123, no. 5: 405-413.

Molenaar, A. A. A., A. Scarpas, X. Liu, and S. M. J. G. Erkens. 2002. "Semicircular bending test: simple but useful?" *Journal of the Association of Asphalt Paving Technologists*, 71: 794-815.

Mukhtar, M. T. and B. J. Dempsey. 1996. "Interlayer stress absorbing composite (ISAC) for mitigating reflective cracking in asphalt concrete overlays." *Final Report, Transportation Engineering Series No. 94*, Cooperative Highway and Transportation Series No. 260, University of Illinois, Urbana, IL.

Seo, Y., Y. R. Kim, and M. W. Witczak. 2002. "Application of the digital image correlation method to mechanical testing of asphalt-aggregate mixtures." *Transportation Research Record* 1789: 162-172.

Slevadurai, A. P. S., M. C. Au, and W. A. Phang. 1990. "Modeling of low-temperature behavior of cracks in asphalt pavement structures." *Canadian Journal of Civil Engineering*, 17: 844-858.

Song, S. H., G. H. Paulino, and W. G. Buttlar. 2006. "A bilinear cohesive zone model tailored for fracture of asphalt concrete considering viscoelastic bulk material." *Engineering Fracture Mechanics*, 2829-2847.

Song, S. H., M. P. Wagoner, and G. H. Paulino. 2008. "δ25 crack opening displacement parameter in cohesive zone models: experiments and simulations in asphalt concrete." *Fatigue and Fracture of Engineering Materials and Structures*, 31: 850-856.

Souza, F. V. and L. S. Castro. 2012. "Effect of temperature on the mechanical response of thermo-viscoelastic asphalt pavements." *Construction and Building Materials*, vol. 30: 574-582.

van Rooijen, R. C. and A. H. de Bondt. 2008. "Crack propagation performance evaluation of asphaltic mixes using a new procedure based on cyclic semi-circular bending tests." *Pavement cracking: mechanisms, modeling, detection, testing, and case histories*, CRC Press, 437-446.

Wagoner, M. P., W. G. Buttlar, and G. H. Paulino. 2005. "Disk-shaped compact tension test for asphalt concrete fracture." *Society for Experimental Mechanics*, 45, no. 3: 270-277.

Wagoner, M. P., W. G. Buttlar, G. H. Paulino, and P. Blankenship. 2006. "Laboratory testing suite for characterization of asphalt concrete mixtures obtained from field cores." *Journal of the Association of Asphalt Paving Technologists*, 75: 815-852.

Williams, M. L., R. F. Landel, and J. D. Ferry. 1955. "The temperature dependence of relaxation mechanisms in amorphous polymers and other glass-forming liquids." *Temperature Dependence of Relaxation Mechanisms*, 3701-3707.